FINITE ELEMENT ANALYSIS OF THE HEAT TRANSFER IN FRICTION STIR WELDING WITH EXPERIMENTAL VALIDATION

BY

Natalie Vosloo

AT

The Department of Mathematics and Applied Mathematics of the

Nelson Mandela Metropolitan University

SUPERVISED BY

Supervisor: Prof John Gonsalves

Co-Supervisor: Dr Hannelie Lombard

December 2012

Submitted in fulfilment of the requirements for the degree of Magister Scientiae in the Faculty of Science

The financial assistance of the National Research Foundation (NRF) towards this research is hereby acknowledged. Opinions expressed and conclusions arrived at, are those of the author and are not necessarily to be attributed to the NRF.

FINITE ELEMENT ANALYSIS OF THE HEAT TRANSFER IN FRICTION STIR WELDING WITH EXPERIMENTAL VALIDATION

Acknowledgements

I would like to thank my supervisors, Prof John Gonsalves and Dr Hannelie Lombard for assisting me so greatly in getting my dissertation to what it is today, this would not have been possible without their insight into Applied Mathematics and Engineering. My friends and family deserve my deepest thanks too. It was my mother, Odette, and my sister, Lara, who brought me countless cups of coffee and were my support whenever I needed them at home and my friends, Meredith Barnes, Kelly Mortimer, Kelly Galloway, Rube Geyer, Paul Blake, Liana and Arno Janse van Vuuren, Jenna Snodgrass, Philippa Webb and Christiaan Pretorius who provided much needed encouragement at every opportunity they got. Thank you. This would not have been possible without you. I would like to thank God for the opportunity given to me to study. I continue to pray that I will honour Him with all my gifts and talents.

I would like to acknowledge the National Research Foundation and the Nelson Mandela Metropolitan University for the funding they provided me for this research.

FINITE ELEMENT ANALYSIS OF THE HEAT TRANSFER IN FRICTION STIR WELDING WITH EXPERIMENTAL VALIDATION

Abstract

Friction Stir Welding is a relatively new joining process. The heat transfer involved is crucial in determining the quality of the weld. Experimental data, though important, does not provide enough information about the heat transfer process and experiments can be costly and time consuming.

A numerical model, using the finite element method, was developed to simulate the heat transfer in the workpiece in which the heat generation due to friction and plastic deformation was modelled as a surface heat flux boundary condition. This model was applied to Aluminium Al 6082-T6 and Titanium Ti 6Al-4V for different welding conditions.

Results were validated with experimental results. The model was shown to give better predictions of the maximum temperatures at locations in the workpiece than the overall temperature trend.

A parametric study was also performed on the Aluminium model in order to predict temperature fields of the workpiece for welding conditions that were additional to those undertaken experimentally. It was found that rotational speed had a larger effect on the change in temperature than the feed rate. From the parametric study it was also clear that lower rotational speeds (300 to 660 rpm) had a greater effect on the change in temperature than the higher rotational speeds (840 to 1200 rpm).

It was concluded that the model was well suited for the estimation of temperatures involved in the FSW of Aluminium Al 6082-T6 but was not as accurate when applied to the FSW of Titanium.

Contents

List of Figures

List of Tables

Chapter 1

Introduction

1.1 Background to Friction Stir Welding

Friction Stir Welding (FSW) is a relatively new joining process that was established by Wayne Thomas and co-workers at the Welding Institute (TWI) in 1991 [1] . FSW is referred to as a *solid-state* joining process since the material for the welded plate is not heated above its melting point [1] which makes it ideal for applications where metal characteristics must remain the same, as far as possible after being welded, such as in the marine, automotive and aircraft industries.

Friction Stir Welding has been shown to be a viable method for joining low melting point metals such as Aluminium and Copper [5, 6, 7, 8] and recently there has been a great deal of research in using the technique on harder materials such as Titanium and Steel [2, 9].

An understanding of the FSW process can help in the development of mathematical models which could accurately predict the temperatures occurring in the workpiece during the welding.

As part of a larger model building strategy that aims to develop collection of models capable of analyzing the FSW process to provide engineers with detailed post welding parameters from which optimal welds can be predicted, this study will attempt to lay the foundation by providing an analysis of the heat transfer in Friction Stir Welding. Heat transfer is a crucial element in determining the quality of the weld. In order to validate the model, experimental temperature measurements (discussed further in Section (4)) will be conducted for the FSW of Aluminium alloy Al 6082-T6 and Titanium alloy Ti 6Al-4V plates.

1.2 The Friction Stir Welding Process

FSW involves the joining of two plates or sheets of metal, referred to as the work surface or workpiece, that have been softened along the join or weld line by the means of a rotating tool. The basic schematic of the process is shown in Figure (1-1).

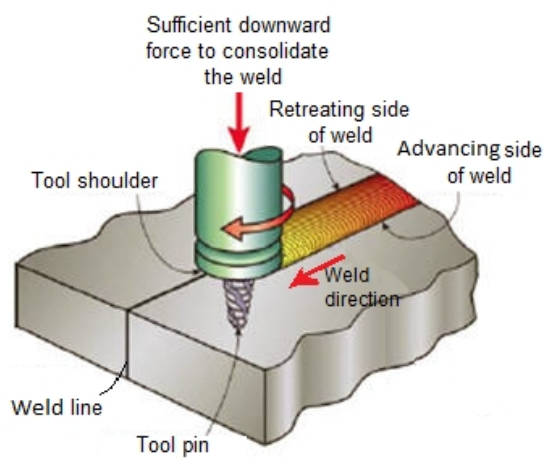

Figure 1-1: Schematic illustrating the process of Friction Stir Welding [1]

For two abutted plates to be joined, the plates need to be clamped with the weld line on

a rigid backing plate in a manner that prevents the plates from separating at the weld line during the weld [10]. FSW takes place in several stages. Firstly, the tool is moved through the air towards the workpiece until contact is made and then the tool is rotated clockwise or anticlockwise. The rotating tool generates frictional heat at the tool-workpiece interface which causes the workpiece to plasticize. The softening of the material allows the tool pin to be plunged into the workpiece until the shoulder is forced against the workpiece surface. After the plunge phase, the tool is allowed to dwell at the entry point, *i.e.* rotate without translational motion, until the workpiece in the local vicinity of the entry point has preheated sufficiently enough to be plasticized. This is done to minimize forces on the tool as translation of the tool commences.

Using either position control or force control [11], the tool is allowed to traverse along the weld line. In this study position control was utilized. Position control utilizes a known plunge depth whereas force control utilizes specified applied forces on the tool such as the downward force, F_z, for example [4]. As the tool begins to move along the weld line, a period of transient heating occurs where the heat generation and temperatures keep changing until a steady-state is reached [12]. The combined translation and rotation of the tool stirs the material wake [13]. The side of the material which moves in the same direction as the translating tool, is called the advancing side (AS) while the side on which the material moves in the opposite direction to translation of the tool is called the retreating side (RS) [14]. In front of the rotating tool, material is mixed from the advancing side to the retreating side, while the reverse happens at the rear of the tool. As the tool leaves an area, the plasticized material cools and solidifies. This solidified material forms the weld. A steady-state thermal stage occurs when the thermal field around the tool remains relatively constant even though there are some fluctuations in the

heat generation. At the point where the tool is allowed to exit the workpiece, a hole, known as a keyhole, is formed [15].

1.3 The Welding Tool

To perform FSW, a welding tool is required. The welding tool consists of a shoulder and a tool pin and is primarily non-consumable during the weld [4]. An example of a welding tool is shown below in Figure (1-2).

Figure 1-2: An example of a FSW tool [2]

Heating of the metal due to friction occurs predominantly under the tool shoulder because of its larger surface area whereas the tool pin is primarily responsible for the stirring action although it also generates some of the heat [12]. The design of the tool, which affects the amount of stirring and friction created at the tool-workpiece interface [13], can vary depending on the desired outcome for the physical properties of the welded material. Some tool designs include tapering or threading of the pin and could include changes to the angle that the shoulder makes with the top of the pin [16]. In some high temperature welding applications the tool pin

is consumed by the weld but in most cases of lower temperature welding such as in Aluminium, the tool pin remains a rigid solid that is neither plasticized nor consumed in the weld [4].

1.4 Controlled Process Parameters

There are a number of process parameters involved in the welding process depending on whether position or force control of the tool is employed. In this study, for reasons which will be discussed later, position control mode will be employed. The following welding parameters are however crucial to this study:

- *Tool feed rate and rotational speed*: The tool feed rate and the rotational speed have a direct result on the heating of the workpiece material [13]. The choice of these two parameters is crucial in providing enough heat generation in order to create a good flow of the material around the tool [17]. Higher rotational speeds generally result in higher temperatures due to the increase in frictional heating [13], whereas temperatures are lowered when the feed rate is increased.

- *Plunge depth*: The lowest vertical depth of the shoulder that is pushed into the material is called the plunge depth. This parameter is important in the prevention of defects such as a *kissing bond* where only a partial bond is formed if the pin does not completely penetrate the weld [17].

- *Tool tilt*: The angle that the spindle makes with the vertical, also called the tool tilt, typically varies from 0° to 4°. The tool can be tilted forwards or backwards and this affects the material flow around and under the tool [18].

1.5 Heat transfer involved in Friction Stir Welding

1.5.1 Introduction

Friction Stir Welding is a coupled thermo-mechanical process in which the material flow around the tool is highly dependent on the heat generated by friction between the tool and the workpiece material [19]. The heat generated by the tool greatly influences the quality of the weld [20, 21]. A weld is considered *good* based on material properties such as the tensile strength of the base metal and the absence of weld defects such as voids, oxidation and tool damage [21]. For Aluminium alloys it has been found that temperatures approaching 80% to 90% of the melting point of the base metal yield a high quality weld [22].

Although welding defects occur more commonly in traditional fusion welding techniques they can also occur during FSW if the heat generated is not ideal [23]. For this reason it is vital to understand the different welding stages to prevent defects in the weld.

1.5.2 Experimental Problems

Since FSW is still a relatively new and complex process, there is still much that is only partly understood. A good understanding of the heat generation process involved in FSW is essential since it affects the weld quality [20, 21]. However, because there are so many factors contributing to it, such as tool design and process parameters, heat transfer is particularly complicated.

With the aid of devices, such as thermocouples and infrared cameras, thermal data from the workpiece can be captured during a weld [12, 24]. Such data does not always provide sufficient information regarding the heat transfer process as a result of thermocouple damage or thermocouple position changes for example. Besides data collection problems, experimental

observations in general are both time consuming and expensive.

To circumvent the need for numerous experiments, many researchers have opted to employ mathematical modelling techniques in order to predict the temperatures in the tool and the workpiece. Mathematical models with analytical solutions exist [25, 12] but they have all been based on the ideal situation. Since many of the material properties, such as specific heat capacity for example, are temperature dependent, this causes the problem to become non-linear. The most practiced and generally accepted approach for solving non-linear problems has been the development of numerical models employing techniques such as the finite difference method (FDM) [12] or the finite element method (FEM) [25, 26, 27]. These numerical models have been developed in order to study, amongst others, the influence of weld parameters on the heat transfer in the workpiece.

1.6 Research Statement

A great deal of research [28, 24, 10] has gone into numerical and experimental studies of heat transfer in FSW in order to obtain a better understanding of the thermal effects of the materials involved. This research was necessary since the heat input into the workpiece material directly affects the microstructure of the welded material and hence the quality of the weld. Experimental thermal data capture, while important, does not provide sufficient information regarding the heat transfer process and is generally expensive and time consuming.

This dissertation will discuss, develop and apply the heat equation to model the heat transfer involved in the FSW process in order to gain a better understanding of the temperature field occurring in the workpiece. A finite element based model of the heat transfer problem, similar

to those developed by a number of researchers, will be modified and extended for this purpose. The model, developed using the software package COMSOL Multiphysics [29], will then be applied to Aluminium Al 6082-T6 and Titanium Ti 6Al-4V and validated using experimentally obtained data. It is envisaged that the model will then provide a helpful tool in predicting possible temperature fields that could occur as a result of specific input process parameters.

1.7 Research Objectives

This study will aim to achieve the following list of research objectives:

- To review the existing FSW literature, with particular reference to implementation and application of thermal models;
- To modify and extend an existing numerical model of the heat transfer of FSW and apply the physical properties of Aluminium Al 6082-T6;
- To investigate whether the model could be readily adapted to the FSW of Titanium Ti 6Al-4V;
- To collect experimental temperature data from welds of Aluminium Al 6082-T6 and Titanium Ti 6Al-4V;
- To validate the numerical model using the experimentally obtained data;
- To document the validity of the numerical model; and
- To indicate future research aspects of the analysis.

Chapter 2

Introduction to Heat Transfer Modelling

2.1 The Heat Equation

The transient heat conduction equation [30, 31] that describes the change in temperature in a domain, Ω over time is given as

$$\rho c \frac{\partial T}{\partial t} = \nabla \cdot k \nabla T + Q \tag{2.1}$$

where the solution, $T(x, y, z, t)$ [K] is the temperature, ρ [kg/m^3] is the material density, c [J/(kg·K)] is the specific heat capacity and k [W/(m·K)] is the thermal conductivity coefficient and Q [W/m^3] is the term defining the internal heat source given by the heat generated per unit volume.

When the analysis is restricted to a steady-state, $\frac{\partial T}{\partial t}$, vanishes and Equation (2.1) becomes the steady-state heat equation given by:

$$-\nabla \cdot k\nabla T = Q \tag{2.2}$$

2.2 Challenges in Heat Transfer Modelling in FSW

The main challenge arising when developing a thermal model that accurately describes the heat transfer process in FSW is that of determining the function that adequately describes the heat generated by the tool. Generally, heat generation can either be modelled as an internal heat source, Q, that forms part of the heat equation or as a heat flux boundary condition where Q is set to zero. It is possible to model heat generation both as an internal heat source as well as a heat flux but this approach is not common in thermal models.

The majority of the heat generated during the welding process is as a result of [12]

- plastic deformation of the workpiece, and
- friction between the tool surface and the workpiece.

Plastic deformation is defined as the permanent change in a shape or structure due to applied stresses that are larger than the yield stress for the material [32].

It is assumed that the contact conditions occurring at the tool-workpiece interface also have a large effect on the heat generation [12]. These contact conditions are related to the temperature dependent viscosity of the workpiece [33] and includes

- the *slipping* condition where the material slips past at the tool-workpiece interface at a lower velocity than the tool,
- the *sticking* or *no-slip* condition where the metal of the workpiece sticks to the tool and has the same local velocity as the tool, or
- a combination of the two.

It is more likely that a combination of the two contact conditions occur since normal contact stresses and temperatures vary over the tool.

To further complicate any thermal model, parameters such as the friction coefficient and tool pressure are difficult to measure [25]. The coefficient of sliding friction is temperature dependent and presently, can only be approximated. Frigaard and co-workers [12], for example, assigned the value of 0.5 for the coefficient of *sticking* friction and 0.25 for *sliding* friction. Generally these values must be obtained experimentally or via an inverse modelling process.

Analytical models [30] can be used to predict the temperatures in ideal situations but their usefulness diminishes when real problems are examined. This together with the fact that many model parameters are temperature dependent means that the process is non-linear requiring the development of numerical models.

In this study a simple thermal model will be developed and solved using the (FEM). To simplify the problem, only the steady-state stage of the welding process will be considered. Heat generated will be assumed to be due to plastic deformation only and friction will only be included implicitly. This is done in order to move away from using estimated frictional coefficients in the model.

The following section will review the literature on the heat transfer in FSW, with particular

reference to thermal modelling.

2.3 Literature Review

2.3.1 Introduction

A variety of numerical models have been developed where the workpiece is either modelled as a solid [21], a viscoplastic material [34, 35] or as a non-Newtonian fluid [3, 36]. In some models the rotating tool moves through the workpiece as a moving heat source [12, 37] while in others, the tool is assumed to be stationary while the workpiece moves [38]. The choice of whether the tool is moving or stationary affects the governing equation.

If the tool moves then heat generation is typically described by an internal heat source with non zero Q, whereas if the tool is assumed to be stationary and the workpiece moves then the heat generated is introduced through surface heat fluxes and Q is set to zero [39]. The latter choice is generally associated with a symmetric weld line which has the added affect of reducing the domain size.

Based on various assumptions made about the FSW process, the models discussed in the next section have been divided into three categories, namely: thermal models, thermo-mechanical models and thermal fluid models. Thermal models solve only the heat equation whereas, thermo-mechanical models solve the heat and equilibrium equations and lastly, thermo-fluid models solve the heat, equilibrium and continuity equations. Purely thermal models in FSW are not common as many researchers either incorporate the residual stresses in the process or the flow of the material about the pin. Residual stresses are those that remain in a material after the forces have been removed and often result in deformation of the material [40].

Although the work in this dissertation will focus on a purely thermal model, where thermo-mechanical or thermo-fluid models add to the body of knowledge concerning heat flow, they have been included.

A few models in each of the three categories will now briefly be discussed.

2.3.2 Thermal Models

Thermal models attempt to solve the transient or steady-state heat equation with an appropriate set of initial and boundary conditions (IC's and BC's) in order to obtain useful information about the temperature field generated by the rotating tool. These models differ in their focus and the methods used for their implementation.

A great deal of research has gone into the derivation of the heat generation term as either an internal source or as a surface flux, since it is affected by many complicating factors such as the contact conditions at the workpiece-tool interface.

A solid foundation for future research was given by Maalekian and co-workers [39] in a paper which compared the different heat generation terms. Three different heat sources were modelled and the results were compared against experimental data to determine the most accurate approach. The first two models were based on analytical results with the first using heat generation due to constant Coulomb friction while the second using heat generation due to friction and plastic deformation. Both these models were found to be very practical for quick, but rough, estimations of the heat input and only slightly less inaccurate than the third method when the results were compared with experimental data. For the third method, the heat generation term $Q(t)$ was found from experimental measurements by minimizing the least squares function of the predicted temperature values and the measured temperature values.

Both the finite difference method and the finite element methods were employed to solve the heat equations.

One of the most well known derivations of the heat generation term is that by Frigaard and co-workers [12] who derived the heat generation term, Q [W/m^3] as a function of the interfacial torque required to rotate a circular shaft relative to the plate surface. The following expression was obtained for the internal heat generation term

$$Q = \frac{4}{3V}\pi^2 \mu P N R^3 \tag{2.3}$$

where V is the unit volume [m^3], μ is the coefficient of friction, P is the pressure across interface [N/m^2], N is the rotational speed [rad/s] and R is the surface radius [m].

Two different approaches were then used to apply this heat generation to the model. Firstly, the heat source was modelled as a moving point source and secondly, as a line source at one instant in time. The heat equation was solved employing a stationary workpiece and a moving tool. The value of the temperature dependent coefficient of friction, μ, was found experimentally to range between 0.25 for *sliding* friction and 0.5 for the *sticking* friction condition. A value of $\mu = 0.4$ was selected for partial *sliding* and *sticky* friction. The heat equation was then solved for the transient temperature field in the workpiece using FDM. The tool was not included in the analysis.

Like Frigaard and co-workers, Rajamanikam [20] employed a simple heat conduction model for the workpiece and excluded the tool. Heat generation was assumed due to friction only with $\mu = 0.4$, the value obtained by Frigaard and co-workers [12]. The model geometry was assumed to be symmetric about the weld line with the heat source moving along the surface and weld

line.

Chao and co-workers [21] modelled heat flow in both the workpiece and the tool. The model incorporated a steady-state analysis of the heat transfer in the tool and then used transient analysis when modelling the heat transfer in workpiece. The heat generation term was obtained from experimental data.

Examples of studies where the heat is modelled as heat flux boundary conditions instead of a heat source term can be found in Hattel and co-workers [25] and Song and Kovacevic [38].

Hattel and co-workers [25] introduced a thermal model that included mechanical effects without having to solve for any mechanical fields. For the derivation of the heat flux term, the fact that the contact stress must be in equilibrium with the material yield shear stress of the underlying material for steady-state conditions, yielded the following relationship

$$\tau_{friction} = \tau_{contact} = \tau_{yield}(T) \tag{2.4}$$

where $T = T(x, y, z)$ is the non-uniform temperature at the contact interface. The heat generation coming from friction was now described using the material's yield stress rather than the more commonly used Coulomb approach which utilizes the non-uniform pressure distribution and an estimated coefficient of friction. Some of the advantages of using the shear stress as opposed to the Coulomb friction are the following:

- more data is available for the material's yield shear stress as opposed to the friction coefficient, and

- prior knowledge of the pressure system is not needed.

The heat contributed by both friction and plastic deformation were given by the following surface fluxes

$$q_{friction} = (1-\delta)\omega r \tau_{friction} \tag{2.5}$$

$$q_{plastic} = \delta \omega r \tau_{yield} \tag{2.6}$$

where δ is equal to 1 for the *sticking* condition and zero for the *sliding* condition. Combining this with Equation (2.4) and assuming pure shear yielded the expression for the total heat generation surface flux, q [W/m^2], given by:

$$q = \omega r \tau_{yield}(T) = \omega r \frac{\sigma_{yield}(T)}{\sqrt{3}} \tag{2.7}$$

where ω is angular velocity of the tool [rad/s], r is the radial distance from the centre of the tool pin [m], τ_{yield} is the maximum temperature dependent yield stress [N/m^2] and σ_{yield} is the temperature dependent shear stress [N/m^2]. Since the heat flux term, q is now temperature dependent, the problem becomes nonlinear, leading to an increase in computational effort.

Song and Kovacevic [38] simplified the difficult task of modelling the moving tool by placing the coordinate system on the tool thus ensuring a stationary tool and a moving workpiece. Unlike the majority of researchers, they employed the (FDM) to solve the heat equation which now included an artificial convection term, reflecting the moving workpiece

$$\rho c \frac{\partial T}{\partial t} + v_{weld} \rho c \frac{\partial T}{\partial x} = \nabla \cdot k \nabla T \tag{2.8}$$

where v_{weld} is the translational speed of the tool in the positive x direction.

To simplify the model, they included symmetry about the weld line, an unthreaded tool pin and heat generation at the shoulder-workpiece interface caused only by friction. Further, the heat generation was assumed to be zero when the temperature of the workpiece reached the melting point of the material being welded.

The heat flux at the shoulder-workpiece boundary was given by

$$q_s = 2\pi \mu F_n N r \tag{2.9}$$

where μ is the coefficient of friction, F_n is the normal force [N], N is the rotational speed [rad/s] and r is the radial distance from the center of the tool pin to calculation point [m].

2.3.3 Thermo-mechanical Models

Thermo-mechanical models are used to predict temperature and residual stresses in the FS welds. Temperature is solved for in the heat equation while deformation and mechanical fields are obtained by solving the Cauchy equations of motion together with the constitutive equations. These equations are either solved together as a coupled problem or separately where the heat equation is solved first and the resulting temperature field is used as a set of initial conditions for the motion and constitutive equations.

The governing equations for thermo-mechanical models are given by

- the heat equation: Equation (2.1);

- Cauchy equations of motion, an expression of Newton's second law:

$$\rho\ddot{\overline{u}} = \nabla \cdot \boldsymbol{\sigma} + \overline{F} \tag{2.10}$$

- Constitutive equations, general form of Hooke's Law describing the relationship between stress and strain:

$$\boldsymbol{\sigma} = \mathbf{C} : \boldsymbol{\varepsilon} \tag{2.11}$$

- Strain-displacement equations:

$$\boldsymbol{\varepsilon} = \frac{1}{2}\left(\nabla\overline{u} + (\nabla\overline{u})^T\right) \tag{2.12}$$

where ρ is the mass density [kg/m^3], $\overline{u}$ [m] is the displacement vector, $\boldsymbol{\nabla}\cdot(\cdot)$ is the divergence operator, $\boldsymbol{\sigma}$ [N/m^2] is the Cauchy stress tensor, $\overline{F}$ [N/m^3] is the body force per unit volume vector, $\boldsymbol{C}$ [N/m] is the fourth order stiffness tensor, $\boldsymbol{\varepsilon}$ is the infinitesimal strain tensor. $\nabla(\cdot)$ is the grad operator and $\boldsymbol{A} : \boldsymbol{B} = \boldsymbol{A}_{ij}\boldsymbol{B}_{ij}$ is the inner product of two second order tensors.

The heat equation for thermo-mechanical problems differs from that used in purely thermal models in that the choice of the heat generation term, Q, involves the material characteristics of the workpiece.

Instead of modelling the workpiece as a solid as done previously in thermal models, Chen and Kovacevic [26] developed a thermo-mechanical model based on the assumption that the workpiece was a ductile material with defined elasticity, plasticity and kinetic hardening. The tool was assumed to be a rigid solid. Heat generation was due to friction with a constant coefficient of friction and a constant shear stress. The model could also be utilized to optimize

the FSW process by minimizing the residual stress in the weld.

Kim and co-workers [41] formulated their thermo-mechanical problem in the Eulerian frame of reference. Full thermal BCs were implemented to incorporate the effect of the backing plate which is not included in many models. Heat generation was assumed to be due to plastic deformation only and did not include friction. The geometry was considered asymmetric and had different expressions for the inflow and outflow velocities around the tool pin. Yield stress was temperature dependent and a full sticking condition was applied at the tool-workpiece interface.

Although the work discussed in this section is very informative with regards to the temperatures and residual stresses involved in FSW, an obvious limitation to the modelling is the lack of the ability to describe the material flow which could also play an important role in the heat transfer process involved. It is a logical step to model the plasticized material as a non-Newtonian fluid in order to capture the material flow and the temperature field in the workpiece. In Section (2.3.4) thermo-fluid models are discussed in more detail.

2.3.4 Thermo-fluid Models

Thermo-fluid or Computational Fluid Dynamical (CFD) models, use the assumption that the material of the workpiece in FSW is a highly viscous incompressible non-Newtonian fluid rather than a rigid solid.

Fluids are classified according to their physical properties. A Newtonian fluid, by definition, has its stress directly proportional to its strain. The proportionality constant for the stress-strain curve is the viscosity of the material [42]. In FSW, however, the workpiece material has a viscosity that is not constant since it varies with temperature and so the workpiece is modelled

as a non-Newtonian fluid. The governing equations for CFD models are the heat or energy and Navier-Stokes equations. The Navier-Stokes equations consist of the continuity equation and the momentum equations for fluids. The governing equations for thermo-fluid models are as follows:

- Heat equation with an added convective term:

$$\rho c \left(\frac{\partial \overline{v}}{\partial t} + \overline{v} \cdot \nabla \overline{v} \right) = \nabla \cdot k \nabla T + Q \tag{2.13}$$

- Continuity equation for incompressible fluids:

$$\nabla \cdot \overline{v} = 0 \tag{2.14}$$

- Momentum equation for fluids:

$$\rho \left(\frac{\partial \overline{v}}{\partial t} + \overline{v} \cdot \nabla \overline{v} \right) = -\nabla P + \eta \nabla^2 \overline{v} + \overline{F} \tag{2.15}$$

where ρ [kg/m^3] is the density, $\nabla \cdot \overline{v}$ is the divergence of the velocity of the fluid, $\overline{v}$ [m/s], $\boldsymbol{Q}$ is the volumetric heat source [W/m^3], P [N/m^2] is the pressure, η [N·s/m^2] is the constant dynamic viscosity and $\overline{F}$ [N/m^3] represents body forces such as gravity or centrifugal forces.

In this section the focus falls on the work by Colgrove and co-workers [3, 28], Qin [34] and Nandan and co-workers [35, 43]). Of particular importance is the work by Colgrove and Shercliff [3] as the models, developed using COMSOL Multiphysics [29], generally influenced the modelling approach for this study. In this model, the tool was assumed to be a stationary solid

while the workpiece material was allowed, by means of a moving mesh, to flow past. The model assumed a full *sticking* condition at the tool-workpiece interface with the workpiece velocity equal to the rotational velocity of the tool. Heat generation was hence due only to plastic deformation and friction was not included since there was no *sliding* contact condition. The model schematic is shown in Figure (2-1) and includes a fully coupled thermal/flow analysis in Region **C** around the tool where both the material flow (momentum and continuity) and heat equations were solved. Full thermal boundary conditions at the backing plate and tool were incorporated as well as convection at the top and bottom surfaces. Region **A** was assumed to be a solid because of its distance from the plasticized area. In this region only the heat equation was solved.

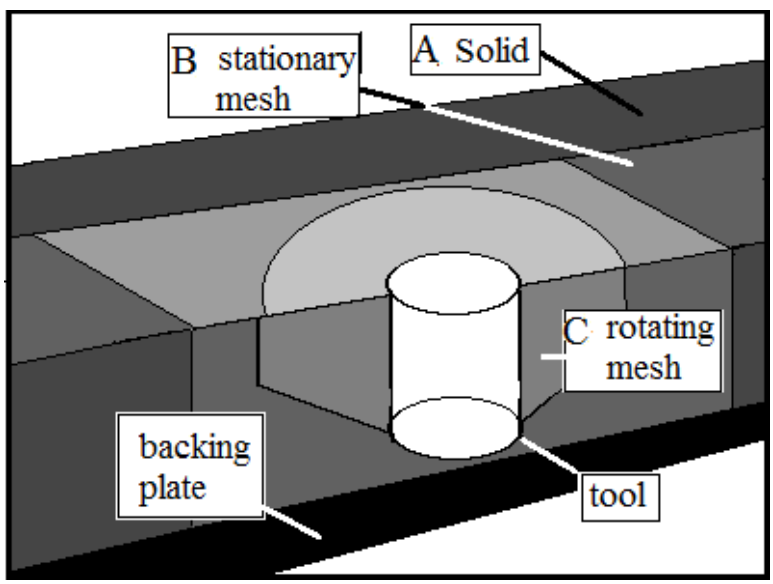

Figure 2-1: A CFD model diagram [3]: Region A: heat conduction in a solid; Region B: Stationary mesh; Region C: fully coupled thermal/flow analysis

This work was later modified [28] to include a two-stage approach, common to many CFD models. In stage one, the temperature gradient is determined which then is used as an initial

condition for the second stage of the model. Firstly, a three-dimensional heat transfer model of the region around the tool was developed to obtain the temperature gradient field around the tool. During this stage, the translation of the tool was captured. The average temperature around the tool was then calculated and used in the second stage which was simplified to a stationary state two-dimensional axisymmetric CFD model where it was no longer necessary to incorporate the translation of the tool. The model, developed using COMSOL Multiphysics [29], ignored the tool thread feature of the tool. The material was modelled as being a purely plastic material with no elastic properties where flow strength is highly dependent on viscosity. The *sticking* condition was incorporated by allowing the velocity of the material at the tool-workpiece interface to be equal to the rotational velocity of the tool and zero at the exterior boundaries of the weld zone that did not come into contact with the workpiece.

Another two stage CFD model was developed by Qin [34], modelling the workpiece as an elastic-viscoplastic material. The workpiece was divided into two broad rings, the smallest one surrounding the tool, while the second enclosing both the tool and the first ring. In the first stage of the model, the region closest to the tool pin was modelled as a thermo-viscoplastic material. The thermo-viscoplastic solution was then used as the initial condition for the second stage where the outer ring was then modelled as an elastic-viscoplastic material. Heat generation was due to friction and plastic deformation. The *sticking* condition was applied to the pin, while only a slight sticking condition was applied to the shoulder. The two dimensional geometry was considered asymmetric with an inlet boundary and an outlet boundary.

Nandan and co-workers [43] used a three dimensional geometry and solved the steady-state Navier-Stokes and heat transfer equations for single phase plastic flow as a thermo-mechanically coupled problem. The model did not assume symmetry about the weld line but it did assume

that the total heat generated, Q was due to both the friction at the tool pin-workpiece interface and plastic deformation. The heat generation term, Q was defined as

$$Q = Q_p + Q_{fr} \tag{2.16}$$

where Q_p is the total heat generated due to plastic deformation and Q_{fr}, the total heat generated due to friction. Here Q_p and Q_{fr} are defined by

$$Q_p = (1 - \delta)E_{me}\tau(\omega r - U_1 \sin\theta)\frac{A_r}{V} \tag{2.17}$$

and

$$Q_{fr} = \delta\mu_f P_N(\omega r - U_1 \sin\theta)\frac{A_r}{V} \tag{2.18}$$

where A_r is any small area on the tool pin-workpiece interface [m^2], r is the radial distance from the tool axis to the center of the area [m], V is the control-volume enclosing the area A_r, δ is the spatially variable fractional slip between the tool and the workpiece interface, E_{me} is the mechanical efficiency, τ is the maximum yielding shear stress [N/m^2], μ_f is the spatially variable coefficient of friction, P_N is the normal pressure on the surface [N/m^2], ω is the angular velocity [rad/s], v_{weld} is the tool trajectory speed [m/s] and θ [rad] is the angle from the tool trajectory line to the position vector of the area A_r.

When $\delta = 0$, a full *sticking* condition is indicated and the heat is generated by plastic deformation alone. When $\delta = 1$, however, there is a full slip condition which ensures maximum friction heat generation and no heat generated due to plastic deformation.

Many recent models utilize the ALE technique in order to better describe the deformation

and translation of the plasticized workpiece material. Zhang and Zhang [44] employed the ALE technique, described by Hirt [45], where the inflow and outflow of the material was modelled using the Eulerian approach in which the mesh did not follow the material. The top and bottom surfaces were assumed to have a sliding condition and were modelled using the Lagrangian view point where the mesh followed the motion of the material. The results provided information about the velocities, stresses and material flow.

Hilgert and co-workers [46] also showed how a transient Arbitrary Lagrangian Eulerian (ALE) [45] analysis could greatly improve results by combining the advantages of both the Eulerian and Lagrangian approaches. This allowed for tracking of particles in the workpiece as well as a reasonably undestorted view of the deformation of the material around the tool. The model captured the temperature history in the tool and workpiece.

2.3.5 Summary

Three types of heat transfer models were discussed in this chapter, namely, thermal, thermo-mechanical and thermo-fluid models. A number of these models have been modified and combined to form the simple purely thermal model used in this dissertation. For example, the Song and Kovacevic model [38] was chosen as a basis since it captures the effect of the motion of the tool without having to include the complications of modelling a moving heat source. In their model the heat generation was modelled as a surface flux boundary condition that depended on the friction involved.

Earlier it was mentioned that the value for the coefficient of friction found by Frigaard and co-workers [12] had been used in a number of the models. The problem with this, however, is the fact that this value was obtained for Aluminium alloys welded at specific welding parameters

and there is very little known about the friction coefficient for other materials and parameter values. It is important to realize that, unfortunately, the coefficient of friction depends on the tool rotational speed [13] which means that including a constant friction coefficient value could decrease the predictive accuracy of the model. In an attempt to produce a model that can be used to simulate the heat transfer in FSW for any alloy under various welding conditions, the effects of friction must be reduced or eliminated completely. For this reason the heat flux equation used in the Song and Kovacevic model [38] was replaced with Equation (2.7) used in the model of Hattel and co-workers [25].

In this model the heat flux equation depends only on the shear stress associated with the workpiece material without having to solve for the mechanical fields. This means that the model remains a purely thermal model, independent of estimated frictional coefficients which could be a source of numerical errors.

Although no models from the thermo-mechanical and thermo-fluid sections were used directly, they did however influence the work in this study. Colgrove's models [3, 28]) in particular were very helpful as examples of COMSOL Multiphysics [29] software applications.

Chapter 3

Numerical Modelling

3.1 Introduction

An approximate solution, employing the finite element method (FEM), will be obtained by implementing the model in COMSOL Multiphysics [29]. In this chapter the heat transfer model used in this study will be described. Thermal equations and associated boundary conditions (BCs) will be described in general and then applied to the specific geometry of the model. The associated weak formulation of the problem, will be developed and the FEM implementation will also briefly be discussed.

This model is a purely thermal model which means that only the heat equation is solved. Mechanical effects are indirectly included in the flux boundary conditions but without having to solve any mechanical or material flow equations. The FEM is employed to solve the heat equation using COMSOL Multiphysics [29] for implementation.

A number of assumptions regarding the material and processes involved have been made, namely, that the workpiece consists of an isotropic homogeneous material, no phase changes or

material flows are included in the stirring of the workpiece material and only the welding stage will be modelled, that is, the plunge and dwell stages will be ignored. The thermal equations involved in the model will now be discussed.

3.2 Thermal Equations

The time independent heat conduction equation has the form

$$0 = \nabla \cdot k\nabla T + Q \text{ for } \bar{x} \in \Omega \subset \mathbb{R}^3 \tag{3.1}$$

where spatially dependent temperature, $T(x, y, z)$ [K] is the solution, $k(T)$ [W/(m·K)] is the temperature dependent thermal conductivity coefficient [47] and Q [W/m^3] is the term defining any internal heat source. Only two kinds of boundary conditions are possible, namely the Dirichlet condition of the form

$$T = T_0 \text{ on } \Gamma_D \tag{3.2}$$

and Neumann conditions of the form

$$-k\nabla T \cdot \hat{n} = q_0 \text{ on } \Gamma_N \tag{3.3}$$

where $\Gamma = \Gamma_D \cup \Gamma_N$ represents the boundary to the domain Ω. The boundary conditions used in the model will be discussed in more detail in Sections (3.3) and (3.5).

As indicated earlier, there are two options when modelling heat generation in FSW[25]. The first is to model the moving tool as an internal heat source [12], while the second option

is to consider the tool as exterior to the domain Ω, providing moving heat flux across the boundary[38]. The latter situation generally assumes a symmetric weld so that the moving tool introduces, amongst others, flux conditions along the symmetry line. While it is possible to model moving boundary heat fluxes the problem is considerably simplified by placing the origin of the coordinate system on the moving tool, that is, the workpiece moves with a stationary tool. The resulting equation, the convection-conduction equation or transport equations becomes

$$\rho c\overline{v} \cdot \nabla T = \nabla \cdot k\nabla T + Q \text{ for } \bar{x} \in \Omega \subset \mathbb{R}^3 \tag{3.4}$$

where the vector $\overline{v}$ represents the tool velocity, ρ [kg/m^3] the material density and c [J/(kg·K)] the temperature dependent specific heat capacity [47]. For this problem to be well-posed, it is reqired that

$$\nabla \cdot \overline{v} = 0. \tag{3.5}$$

To further simplify the problem it will be assumed that the solution has reached steady-state so that a time-independent problem can be solved, that is, the time-derivative is assumed negligibly small and can be omitted.

Remark A transient analysis was carried out with little change to the solution, thus a steady-state analysis was employed in this study.

Heat generation is modelled via a heat surface flux in the boundary conditions rather than an internal heat source, and so Q is set to zero which yields the following equation

$$\rho c\overline{v} \cdot \nabla T = \nabla \cdot k\nabla T \tag{3.6}$$

Assuming the tool moves in the negative x-direction, the velocity vector is defined as follows:

$$\overline{v} = \begin{bmatrix} v_x & v_y & v_z \end{bmatrix}^T = \begin{bmatrix} v_{weld} & 0 & 0 \end{bmatrix}^T \tag{3.7}$$

where v_{weld} is called the tool feed rate.

Heat generation, assumed due to friction and plastic deformation, is incorporated in the material shear stress. The Coulomb friction model is commonly used, requiring pressure distributions and frictional coefficients. In order to move away from these requirements, the heat flux model employed by Hattel and co-workers [25] was used.

The total heat generation due to plastic deformation and friction in terms of a surface flux defined by the following [25]:

$$q = \omega r \tau_{yield}(T) = \omega r \frac{\sigma_{yield}(T)}{\sqrt{3}} \tag{3.8}$$

where the yield shear stress, $\tau_{yield}(T)$ [N/m^2] was interpolated from experimental data for the maximum yield stress for Aluminium Al6082-T6 [48] and for Titanium Ti-6A1-4V [47]. The function of $\tau_{yield}(T)$ [N/m^2] is shown graphically in Figure (3-1) for both materials.

The temperature dependence of the shear stress causes the heat transfer problem to become non-linear which requires an iterative method to solve. COMSOL Multiphysics does this automatically in the solving process.

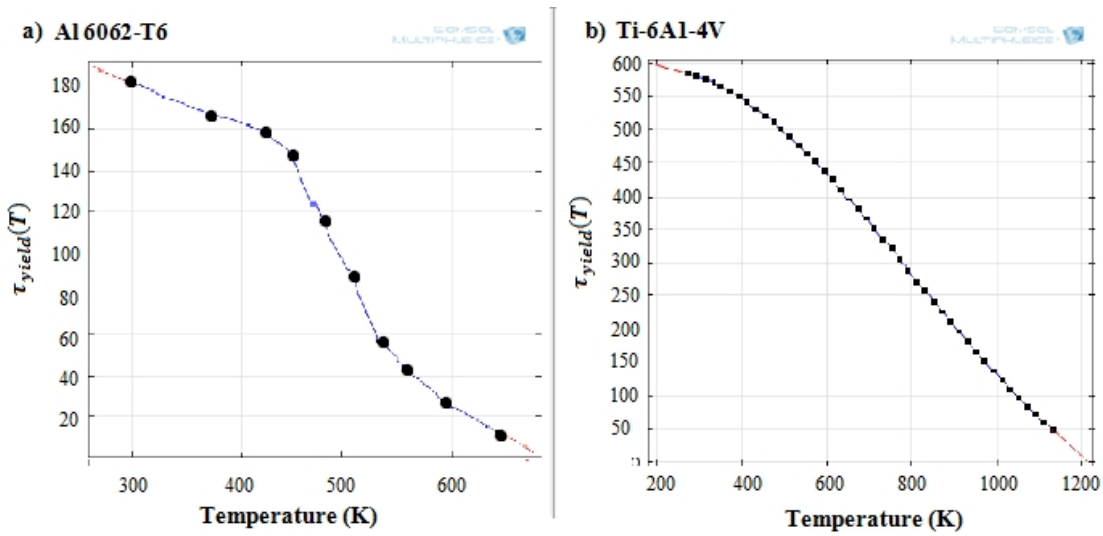

Figure 3-1: a) Temperature dependant Yield Shear Stress curve for Al6082-T6 [48]; b) Temperature dependant Yield Shear Stress curve for Ti-6A1-4V [47]

3.3 Boundary Regions

The boundary of the workpiece domain, Ω, can be represented as the union of distinct boundary regions each corresponding to a different boundary condition. In all the boundary regions, either the temperature (essential BC) or the heat flux (natural BC) is specified. The boundary region on which the temperature is specified is given by:

$$\Gamma_D = \partial\Omega_T \tag{3.9}$$

and the boundary on which the heat flux is specified is given by:

$$\Gamma_N = \partial\Omega_C \cup \partial\Omega_{CR} \cup \partial\Omega_\Phi \cup \partial\Omega_O \cup \partial\Omega_S \tag{3.10}$$

where the boundary regions are presented schematically in Figure (3-2).

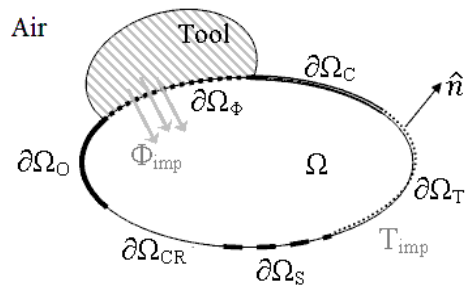

Figure 3-2: Boundary condition regions for the domain

The boundary conditions for the different regions are presented in Table (3.1) below:

Boundary Region	**Description**	**Boundary Type**
$\partial\mathbf{\Omega}_C$	Surfaces in contact with backing plate or clamping	Conduction in solids
$\partial\mathbf{\Omega}_{CR}$	Free surfaces in contact with surrounding air	Convection and radiation
$\partial\mathbf{\Omega}_\Phi$	Surface under tool shoulder and boundary at tool pin	Imposed heat flux from tool
$\partial\mathbf{\Omega}_T$	Side of plate at start of mesh motion	Imposed temperature
$\partial\mathbf{\Omega}_S$	Surface of symmetry or insulation	Symmetry
$\partial\mathbf{\Omega}_O$	Side of plate at end of mesh motion	Outflow

Table 3.1: Boundary descriptions and corresponding boundary conditions

3.4 Model Domain

The model domain consists of the regions where the temperatures are to be determined. In this study we require the temperatures in the workpiece, as generated by the rotating tool pin and shoulder. As heat is supplied to the workpiece from the moving tool in the form of surface

heat fluxes the tool surfaces supplying these fluxes and the workpiece-tool interface need to be identified. Figure (3-3) shows the model domain and identifies a number of important regions.

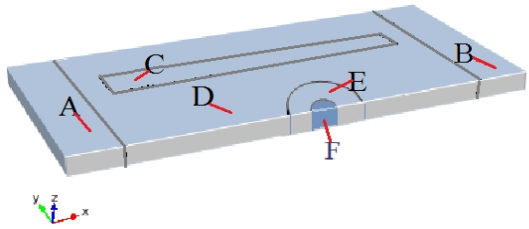

Figure 3-3: Model domain

Region D represents the workpiece and regions A and B represent infinite domains on either side. The length of the workpiece in the x-direction is assumed to be infinite in order to ignore the edge effects that could occur. Region C identifies the region under the clamping bar used to clamp the workpiece to the backing plate. Since the metal in the clamping bar conducts the heat away from the workpiece, it must be identified and suitable boundary conditions implemented. Region E identifies the shoulder surface through which the heat flux enters the workpiece, while region F identifies the tool pin. It is important to note that this region represents the surface in contact with the workpiece only.

The dimensions of the domain are given in Table (3.2).

	Plate (mm)	r_s **(mm)**	r_{p_top} **(mm)**	r_{p_bottom} **(mm)**	h_p **(mm)**
Aluminium	500×120×8	12.75	5	5	8
Titanium	300×120×3	7	4	2	3

Table 3.2: Model Geometry Dimensions for Aluminium and Titanium

where r_s is the shoulder radius, r_{p_top} is the pin radius at the shoulder, r_{p_bottom} is the pin radius at the free end of the pin and h_p is the height of the pin. The tool pin used in the Aluminium model is cylindrical whereas in the Titanium case, the tool pin has a conical shape with the radius equal to 4mm at the shoulder end and 2mm at the bottom free end. In both the Aluminium and Titanium cases, the tool pin was assumed to have a height equal to the thickness of the plate.

Further, a number of assumptions were made about the model geometry in order to lessen the computational effort namely

- The temperature is symmetric about the weld line so that only half of the workpiece needs to be considered;
- The tool tilt is 0°

3.5 Boundary Conditions

In Section (3.3) the various boundary regions were identified (see Figure (3-4)). In this section the relevant boundary conditions to be applied will be discussed in detail.

Figure (3-4) shows the boundary conditions which can be described as follows:

- **Conduction in solids:** Regions C, K and H form the boundary $\partial\Omega_C$ representing conduction from the workpiece to the backing plate (Region H) or clamping bars (Regions C and K). Here the appropriate flux condition is given by

$$-k\nabla T \cdot \widehat{n} = h_{bc}(T - T_{bc}) \tag{3.11}$$

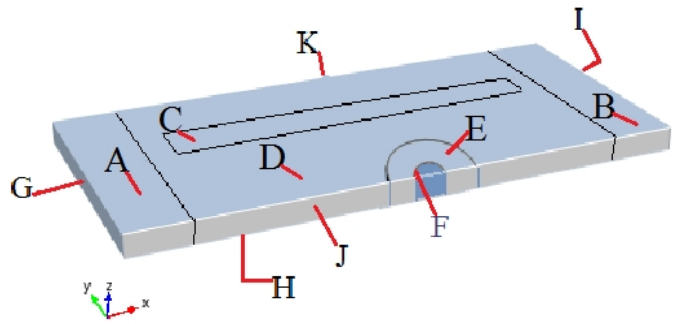

Figure 3-4: Model boundary condition regions

where h_{bc} is the heat transfer coefficient found by Larsen and co-workers [49] and T_{bc} is the initial temperature for both the backing plate and clamping bars. The heat transfer coefficient value used here was assumed to be the same for both Aluminium and Titanium models at the workpiece-backing plate interface due to a shortage of data for Titanium 6Al-4V.

- **Convection and Radiation**: On the free surfaces, Regions A, B and D forming the boundary $\partial\Omega_{CR}$, heat transfer takes place from the plate to the air via convection and natural radiation and is described by the following relationship:

$$-k\nabla T \cdot \widehat{n} = h_{air}(T_0 - T) + \varepsilon\sigma(T_{air}^4 - T^4) \tag{3.12}$$

where h_{air} is the heat transfer coefficient between the plate and the air [31], T_0 is the initial temperature of the plate, ε is the surface emissivity of the plate, σ is the Steffan Boltzman constant and T_{air} is the initial air temperature.

- **Imposed heat flux from tool**: Regions E and F form the boundary $\partial\Omega_{\Phi}$ through which

the heat flux, induced by the tool into the workpiece is imposed. This flux is given by

$$-k\nabla T \cdot \widehat{n} = \Phi_{imp} \tag{3.13}$$

where, at any point (x, y) on $\partial\Omega_\Phi$ experiences a heat flux. The function Φ_{imp} for region E, the surface under the tool shoulder, is defined as

$$\Phi_{imp} = q_{shoulder} = \omega R \tau_{yield}(T) \tag{3.14}$$

where R is the radial distance from the centre of the tool pin to the point, (x, y).

Region F represents the boundary at the tool pin-workpiece interface. Here the imposed heat flux function is given by

$$\Phi_{imp} = q_{pin} = \omega r_p \tau_{yield}(T) \tag{3.15}$$

where r_p is the radius of the tool pin which is constant for the Aluminium model and changes with height for the Titanium model. The yield shear stress function, $\tau_{yield}(T)$ is shown graphically in Figure (3-1) for both materials.

- **Imposed temperature**: Region I forms the boundary $\partial\Omega_T$ and is assigned the initial temperature of the plate at the side where the material enters the computational domain:

$$T = T_0 \tag{3.16}$$

- **Symmetry**: Region J along the weld line surface forms part of boundary $\partial\Omega_S$ and is

assumed to be a symmetry boundary, along which, a symmetry/ insulation boundary condition is applied given by the surface flux

$$-k\nabla T \cdot \widehat{n} = 0 \tag{3.17}$$

- **Outflow**: Region G also forms part of boundary $\partial\Omega_S$ and represents the side where computational mesh leaves the domain. This region is modelled as a symmetry condition utilizing Equation (3.17) in order to keep the temperatures in equilibrium with the temperature at infinity.

3.6 Model Parameters

Table (3.3) gives the model parameters used in both the Aluminium and Titanium models. Here h_{bc} [W/m^{2}K] is the heat transfer coefficient between the workpiece and the backing plate, h_{air} [W/m^{2}K] is the heat transfer coefficient between the workpiece and the surrounding air, ρ [kg/m^3] is the material density, $c(T)$ [J/kg·K] is the specific heat capacity, $k(T)$ [W/m·K] is the thermal conductivity and ε is the thermal emissivity. Both $c(T)$ and $k(T)$ values are specific to AA 6061-T6 since the temperature dependent values for Al 6082-T6 were not available.

Parameter		**Al 6082-T6**	**Ti 6Al-4V**
h_{bc}		415	415
h_{air}		12.25	12.25
ρ		2700	4420
$c(T) = C_0 + C_1T + C_2T^2 + C_3T^3$	C_0	9.29×10^{2}	6.22×10^{2}
	C_1	-6.27×10^{-1}	-3.67×10^{-1}
	C_2	1.48×10^{-3}	5.45×10^{-4}
	C_3	-4.33×10^{-8}	2.39×10^{-8}
$k(T) = C_0 + C_1T + C_2T^2 + C_3T^3$	C_0	2.52×10^{1}	1.92×10^{1}
	C_1	3.98×10^{-1}	1.89×10^{-2}
	C_2	7.36×10^{-6}	-1.53×10^{-5}
	C_3	-2.52×10^{-7}	-1.41×10^{-8}
ε		0.3	0.39

Table 3.3: Model parameters

The tool pin used in the Aluminium model was described with the following material properties, namely the density, $\rho = 7800$ kg/m^3, thermal conductivity, $k = 42$ W/(m.K) and specific heat capacity, $c = 500$ J/(kg.K). The tool pin material for the Titanium model utilized the properties of Tungsten since data for Lanthanated Tungsten was unavailable. These included the density, $\rho = 15770$ kg/m^3 and the temperature dependent specific heat capacity and thermal conductivity given by $c(T) = 0.0001 + 2\times10^{-8}T$ and $k(T) = 158.3 - 0.0661T + 2\times10^{-5}T^2$ respectively.

3.7 Implementation

3.7.1 The Galerkin Finite Element Method

One of the most important advances in applied mathematics in the last century has been the development of the finite element method as a general mathematical tool for obtaining approximate solutions to boundary-value problems. The theory of finite elements draws on almost every branch of mathematics and can be considered as one of the richest and most diverse bodies of the current mathematical knowledge.

To illustrate the method, consider solving the following simple two-point boundary value problem with constant coefficients

$$-pu'' + qu = f \quad \text{on } 0 < x < 1 \text{ such that } u(0) = u(1) = 0$$

where $p > 0$ and $q \geq 0$. We construct a variational problem, firstly defining the residual function, $R \equiv -pu'' + qu - f$, (from where the method of weighted residuals gets its name), then requiring the residual R vanish in the weighted integral sense, that is,

$$\int_{\Omega} v(-pu'' + qu - f)d\Omega = 0,$$

where Ω is the physical domain of interest and v, some suitably defined weighting or test function. To ensure that all integrals are well-defined, we generally restrict $u \in H^2(\Omega)$, where $H^2(\Omega)$ is called a Sobolev space and the weighting function is $v \in L_2(\Omega)$. The regularity requirement (number of continuous derivatives) on the solution u, in the weighted residual method, is dictated by the order of the differential equation.

It is however clear that the weight (test) function v, and solution u, do not come from the same vector space so an effort is made to correct this by distributing the derivatives evenly between both the test and trial functions. This will ensure that both require the same regularity and hence come from the same vector space. This distribution is achieved by using integration by parts (Green's Theorem in higher dimensions) resulting in the following integrals

$$B(u,v) = \int_{\Omega} (v'pu' + vqu)d\Omega,$$

and

$$l(v) = \int_{\Omega} vfd\Omega.$$

Thus the weak formulation is defined as follows: Determine $u \in H_0^1$ such that

$$B(u,v) = l(v) \text{ for all } v \in H_0^1.$$

We are assured that the integrals exist by the requirement that both u and v belong to H_0^1.

The Ritz-Galerkin approximate solution u_h is then defined by resorting to finite dimensional subspace of the Sobolev space $H_0^1(\Omega)$ such that we now determine $u_h \in V_h \subset H_0^1$ such that

$$B(u,v) = l(v) \text{ for all } v \in V_h \subset H_0^1.$$

Assuming that $\dim(V_h) = N$ and that $V_h = span\{\phi_i\}|_{i=1}^N$, the Ritz-Galerkin approximate solution can be expressed as

$$u_h = \sum_{j=1}^{N} c_j \phi_j$$

where the basis function ϕ_i must satisfy the conditions of completeness and linear dependence. Typically polynomials or trigonometric functions are used and defined globally.

In practical situations the determination of suitable basis functions for use in the Ritz-Galerkin method can be extremely difficult, especially in cases for which the domain Ω does not have a simple shape. The Galerkin finite element method overcomes this difficulty by providing a systematic means for generating basis functions on domains of fairly arbitrary shape. What makes this method specially attractive is the fact that these basis functions are piecewise polynomials that are non-zero only on a relatively small part of Ω. Furthermore by discretizing the domain Ω into a finite number E of sub-domains $\Omega^1, \Omega^2, ..., \Omega^E$, called finite elements using node points we are able to generate an interpolatory piecewise polynomial basis.

Employing this basis converts the Ritz-Galerkin approximate problem into an equivalent algebraic problem of the form

$$K\bar{U} = \bar{F},$$

where the stiffness matrix $K_{ij} = B(\phi_i, \phi_j)$ and the load vector $F_i = l(\phi_i)$. The problem is further simplified by the fact that the equivalent matrix and vector are obtained at element level and the the global matrix assembled. This method will now be applied in order to solve the heat equation described in Section (3.2).

3.7.2 Weak Formulation

The strong form of the heat transfer problem, described in Section (3.2) to be solved is: Find $T \in C^2(\Omega)$ such that

$$\rho c\bar{v} \cdot \nabla T = \nabla \cdot k\nabla T \text{ for } \bar{x} \in \Omega \subset \mathbb{R}^3 \tag{3.18}$$

subject to the essential boundary conditions

$$T = T_0 \text{ on } \Gamma_D = \partial\Omega_T$$

and Natural boundary conditions of the form

$$-k\nabla T \cdot \hat{n} = q_0 \text{ on } \Gamma_N = \partial\Omega_C \cup \partial\Omega_{CR} \cup \partial\Omega_\Phi \cup \partial\Omega_O \cup \partial\Omega_S$$

To obtain the weak formulation the space of test functions must be defined, in this case we have

$$U = \left\{ u \in H^1(\Omega) \,|u = 0 \text{ on } \Gamma_D \right\}.$$

Multiply the governing equation by a test (weighting) function $u \in U$ and integrate over the domain Ω. Employing the divergence theorem (integration by parts) to distribute the second partial derivative in the conduction term generates the equation

$$\int_\Omega \left(k\nabla T \cdot \nabla u - \left(\rho c \overline{v} \cdot \nabla T\right) u\right) d\Omega = \int_{\Gamma_N} q_0 u d\Gamma \tag{3.19}$$

Now applying the appropriate boundary conditions to the different sub-regions of Γ_D and Γ_N, Equation (3.19) becomes:

$$\underbrace{\int_{\Omega} \left(k\nabla T \cdot \nabla u - \left(\rho c \overline{v} \cdot \nabla T\right) u\right) d\Omega}_{B(u,T)}$$

$$= \underbrace{\int_{\partial\Omega_C} h_{bc}(T - T_{bc}) u.dS + \int_{\partial\Omega_{CR}} [h_{air}(T_0 - T) + \varepsilon\sigma(T_{air}^4 - T^4)] u.dS + \int_{\partial\Omega_\Phi} \Phi_{imp} u.dS}_{l(u)} \tag{3.20}$$

Thus the weak formulation becomes: Find $T \in V = \left\{T \in H^1(\Omega) \,|T = T_0 \text{ on } \Gamma_D\right\}$ such that

$$B(u,T) = l(u) \text{ for all } u \in U.$$

3.7.3 Stabilization

As mentioned earlier the convection term is introduced in order to model a moving mesh, rather than a moving tool. This unfortunately brings with it its own problems namely an oscillatory solution. To illustrate this problem let us consider the time-independent one-dimensional transport or convection-conduction equation

$$-u'' + \nu u' = 0 \quad \text{on the interval } (0,1),$$

where u could represent the temperature and ν the ratio of velocity and thermal diffusivity. We shall assume $\nu > 0$ and that the solution satisfies boundary conditions,

$$u(0) = 0 \quad \text{and} \quad u(1) = 1.$$

Using N piecewise linear (Lagrange) elements, the assembled finite element model equations can be expressed in the form

$$\frac{1}{h}\left[\left(-1-\frac{\nu h}{2}\right)U_{i-1}+2U_i+\left(-1+\frac{\nu h}{2}\right)U_{i+1}\right]=0; \quad i=2,3,...,N.$$

with boundary conditions $U_1 = 0$ and $U_{N+1} = 1$ It is assumed that the N linear elements are uniform in size such that each element has length $he = h$.

To solve this difference equation we assume that U_i is proportional to r^i and substituting into the above yields the characteristic equation

$$cr^2 + (-a-c)\,r + a = 0$$

from which we get $r = 1$ or $r = \frac{a}{c}$, thus the general solution to the difference equation is

$$U_i = \left(\frac{1-\left(\frac{a}{c}\right)^{i-1}}{1-\left(\frac{a}{c}\right)^{N}}\right).$$

Let us now distinguish the following three cases :

(i) Case $c < 0$: Since $a < 0$ we have $\left(\frac{a}{c}\right) > 0$, thus if $\frac{a}{c} > 1$ then U_i is positive. Thus if $0 < \frac{a}{c} < 1$ we have that, since both the numerator and denominator are negative, U_i is positive.

(ii) Case $c > 0$: Since $a < 0$ we have $\left(\frac{a}{c}\right) < 0$. However, $a + c = -b$ with $b > 0$ so that $c < -1$ which gives $\left(\frac{a}{c}\right) < -1$ we have that U_i is alternately positive and negative : If $U_i > 0$ then $U_{i+1} < 0$, if $U_i < 0$ then $U_{i+1} > 0$. The approximate solution shows an oscillatory

behaviour.

(iii) Case $c = 0$: In this case the difference equations reduce to aU_{i-1} and not on U_{i+1}.The solution will thus be identically zero except for $U_{N+1} = 1$.

Thus, if $c < 0$, then $U_i > 0$ and no oscillations occur; if $c > 0$, then U_i oscillates between positive and negative values; and if $c = 0$ the solution vanishes everywhere except at the point x_{N+1} with $U_{N+1} = 1$. No oscillations occur, but the solution is quite inaccurate.

This means that in order to suppress the oscillations, we must select our element length h such that

$$c = -1 + \frac{\nu h}{2} < 0 \quad \text{or} \quad h\nu < 2.$$

This is a severe restriction on the choice of element sizes when ν is very large. This problem is well known to researchers and arises from the fact that the Galerkin finite method, with linear elements, causes a first derivative to be replaced by a standard central difference formula. The general approach to generating an oscillation-free solution is to use an upwinding scheme [50]. COMSOL Multiphysics [29] software applies both consistent and inconsistent stabilization. In the case of consistent stabilization one of two methods is applied namely, streamline diffusion and crosswind diffusion. Consistent stabilization methods do not perturb the original transport equation. The consistent stabilization methods are used when fluids and solids have translational motion. A stabilization method is active when the appropriate check box is selected. For example, streamline diffusion is active by default and should remain active for optimal performance for heat transfer in fluids or other applications that include a convective or translational term. Because COMSOL Multiphysics [29] bases the discretization of the equations on the finite element method, it provides an elegant way of adding artificial diffusion without actually

perturbing the original equations. This method is more commonly known as the streamline upwind Petrov-Galerkin method (SUPG).

In sections (3.2) and (3.6) it was mentioned that the boundary flux employed by Hattel and co-workers [25] as well as the thermal conductivity and specific heat capacity are temperature dependent. Now a problem is said to be nonlinear if any coefficient or material property is a function of the dependent variable, in this case temperature T. Thus by employing these equations the problem is now nonlinear, that is, the stiffness matrix is now a function of temperature. This together with the mesh translation greatly adds to the overall complexity of the analysis. Fortunately COMSOL Multiphysics [29] has built in methods to handle such difficulties.

3.7.4 Nonlinear Solvers

Consider a system of nonlinear equations in the form of the residual,

$$\overline{R}(\overline{U}) = K(\overline{U})\overline{U} - \overline{F} = \bar{0}.$$

Now assume that we can approximate $\overline{R}(\overline{U})$ by a linear function $\overline{M}(\overline{U};\overline{U}^n)$ in the vicinity of $\overline{U}^n$ as follows:

$$\overline{M}(\overline{U};\overline{U}^n) = \overline{R}(\overline{U}^n) + J(\overline{U}^n) \cdot (\overline{U} - \overline{U}^n)$$

where $J = \bigtriangledown\overline{R}$ is the Jacobian of $\overline{R}$. If $\overline{R} = (R_1, R_2, ..., R_m)^T$ and $\overline{U} = (u_1, u_2, ..., u_m)^T$, entry (i, j) of J equals $\partial R_i/\partial u_j$. To find the next approximation $\overline{U}^{n+1}$ from $\overline{M}(\overline{U};\overline{U}^n) = \bar{0}$, we have to solve a linear system with J as the coefficient matrix. The concept of using a relaxed solution may also be applied to Newton's method. The computational steps can be summarized in the

following algorithm.

Guess a solution $\overline{U}^0$ for the solution of $\overline{R}(\overline{U}) = \bar{0}$.

For $k = 0, 1, 2, ...$until the termination criterion is satisfied.

Solve the linear system $J(\overline{U}^k) \cdot (\overline{U}^* - \overline{U}^k) = -\overline{R}(\overline{U}^k)$ for $\overline{U}^*$.

Set $\overline{U}^{k+1} = \beta\overline{U}^* + (1-\beta)\overline{U}^k$

Next k

NOTE: Calculation of the inverse $J^{-1}(\overline{U}^k)$ is never performed as the cost is simply prohibitive for large systems of equations.

Relevant termination criteria for this method are

$$\left\|\overline{U}^{k+1} - \overline{U}^k\right\| \leq \epsilon_u \text{ or } \frac{\left\|\overline{U}^{k+1} - \overline{U}^k\right\|}{\left\|\overline{U}^k\right\|} \leq \epsilon_r$$

or

$$\left\|\overline{R}(\overline{U}^{k+1})\right\| \leq \epsilon_r \text{ or } \frac{\left\|\overline{R}(\overline{U}^{k+1})\right\|}{\left\|\overline{R}(\overline{U}^0)\right\|} \leq \epsilon_r$$

and where two different tolerances may be used depending on the situation. The weakness of Newton's method arises from the need to compute and invert the Jacobian matrix $J_k = J(\overline{U}^k)$ at each step. The nonlinear solver in COMSOL Multiphysics is an invariant form of Newton's method in which the discrete equations are expressed in the form as $\bar{R}(\bar{U}) = \bar{0}$, where $\bar{R}(\bar{U})$ is the residual vector and $\bar{U}$ is the solution vector. Starting with the initial guess $\bar{U}^0$, the software forms the linearized model using $\bar{U}^0$ as the linearization point. It solves the discretized form of the linearized model $J(\overline{U}^n) \cdot \delta\bar{U} = -\overline{R}(\overline{U}^n)$ for the Newton step $\delta\bar{U} = (\overline{U}^{n+1} - \overline{U}^n)$ using the

selected linear system solver. It then computes the new iteration

$$\overline{U} = \overline{U}^n + \lambda \delta \bar{U},$$

where λ is the damping factor. A value of $\lambda = 1$ results in Newton's method, which converges quadratically if the initial guess $\bar{U}^0$ is sufficiently close to a solution. In order to enlarge the domain of attraction, the solver chooses the damping factors judiciously. Nevertheless, the success of a nonlinear solver depends heavily on a carefully selected initial guess. Thus you should spend considerable time providing the best value for $\bar{U}^0$, giving at least an order of magnitude guess for different solution components.

COMSOL Multiphysics [29] automatically detects nonlinearities, so you normally do not need to decide whether to use a linear or a nonlinear solver. The automatic detection works through analysis of the variables contributing to the residual Jacobian matrix and the constraint Jacobian matrix. If the algorithm finds that both these matrices are complete and do not depend on the solution, the stationary solver and the parametric solver use the linear solver. Otherwise, they use the nonlinear solver. Complete here means that the algorithm only found contributing variables for which the correct Jacobian will be computed.

3.7.5 Discretization

The domain identified in Section (3.4) is now discretized into a finite number of subdomains called finite elements. This was done using the COMSOL Multiphysics mesh generator. The mesh was specified to be very fine near the tool where the temperature gradients were predicted to be very high and coarser at further distances to the tool. The element types were determined

automatically by the software and included prism, hexahedral, triangular, quadrilateral, edge and vertex elements. All elements in the Aluminium model had a minimum size of 0.12 mm and a maximum size of 12mm while those in the Titanium model ranged from 0.8 mm to 8 mm in size. The geometry mesh is shown in Figure (3-5).

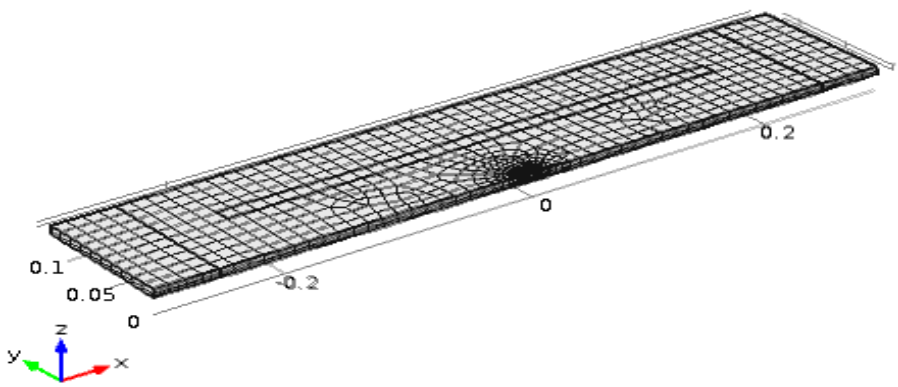

Figure 3-5: Computational mesh

Chapter 4

Experimental Data Acquisition

4.1 Introduction

This section will describe the experiments undertaken to validate the FEM model in this dissertation. This chapter will describe the weld platform, the welding tool, backing plate, clamping mechanism as well as the welding parameters used to obtain the Friction Stir welds. The thermocouples used to measure the temperature will also be discussed as well as their calibration and positions in the workpiece.

4.2 FSW Platform

The FSW platform used to produce all welds is the I-STIR Process Development System (PDS) platform, shown in Figure (4-1). The set up and operation of the machine was carried out using a remote station control pendant connected to a closed loop MTS digital control system. The I-STIR PDS is a 4-axes machine which includes the X-, Y-, Z- and Pitch-axis which are also shown in Figure (4-1). The Pitch-axis controls the tool tilt whereas the other axes control the

vertical and horizontal motion of the spindle. The platform can be operated in either position or force mode. For the welds in this research, only the position control mode was utilized.

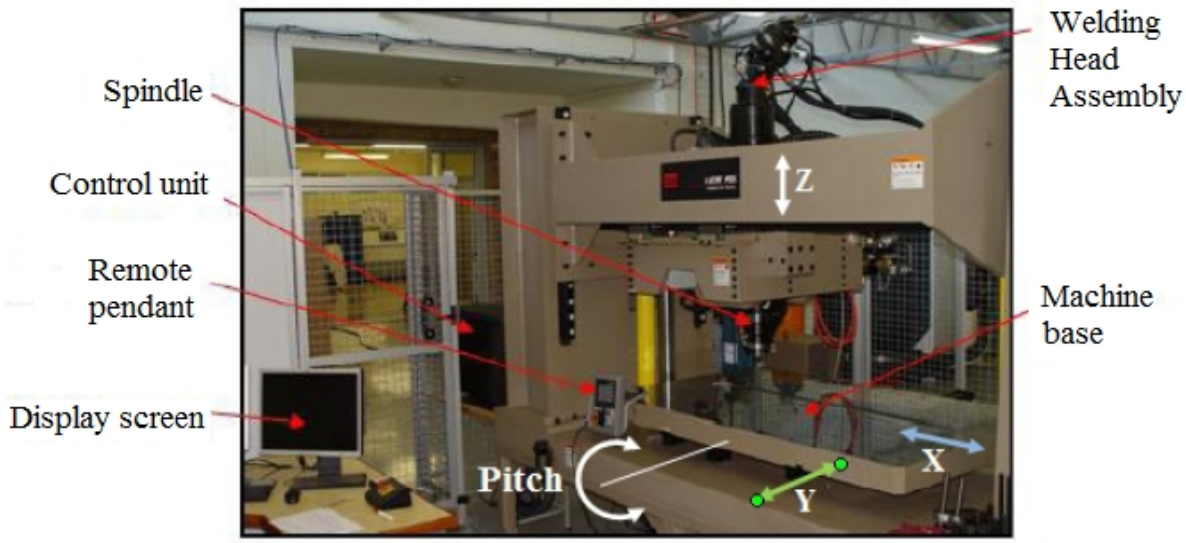

Figure 4-1: I-STIR PDS used in this research [4]

Before FS welding can commence, the spindle must be checked for concentricity and aligned with the center line of the weld. This process is then repeated in order to determine whether the FSW tool is concentric with the spindle.

4.3 Thermal Data Collection Instrumentation

Twelve holes were drilled into the plates on the advancing side of the weld which were used as the positions for the inserted thermocouples. They were all drilled from the top to mid thickness of the plate so that the thermocouples could easily be inserted once the workpiece was clamped. K-type thermocouples were used to measure the temperature of the workpiece during the welds since the associated temperature range (-200 ^{o}C to 1250 ^{o}C) was wide enough

to contain the expected maximum temperatures reached during welding for both Aluminium and Titanium. The accuracy of K-type thermocouples ranges from ±1.5 ^{o}C at 200 ^{o}C to ±9.0 ^{o}C at 1200 ^{o}C. The tips of the thermocouples were placed in the holes in the workpiece, as shown in Figure (4-2), and the Copper plugs at the back of the thermocouples were plugged into a Temp Point data logger with the capacity for 31 thermocouples which was then linked to a PC. The software used for the thermocouple calibration before the welding, and temperature data logging during the welding was the DataTemp Multidrop Rev.5.3.1 Data Translation.

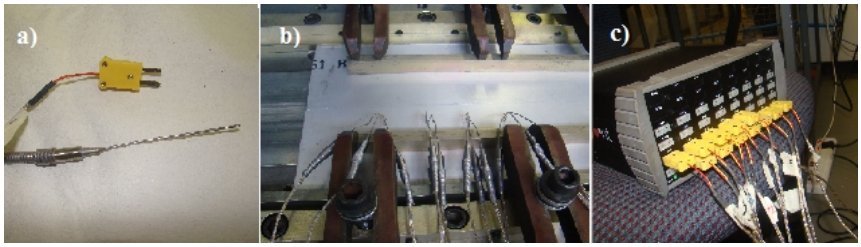

Figure 4-2: a) K-type thermocouple with temperature gage on the one end and electric plug on the other; b) Thermocouple tips inserted into holes in workpiece; c) Thermocouple plugs inserted into channels in Temp Point data logger

Before the welding commenced the thermocouples were placed with the tips in the holes as described above and then individually calibrated to the plate temperature which was measured using a portable thermocouple. Data recording began once the tool was lowered into the position where the tool pin was in contact with the workpiece. A data sampling rate of one-tenth of a second was employed. The experimental results will be discussed in Section (5).

4.4 Aluminium Al 6082-T6 Friction Stir Welds

4.4.1 The Friction Stir Welding Tool

The tool used to weld the 8 ±0.2 mm thick Aluminium Al6082-T6 plates is shown in Figure (4-3). The tool consisted of a flat cylindrical shoulder with a radius, $r_s = 12.75$ mm and an unthreaded cylindrical pin with a length, $h_p = 7$ mm and a radius, $r_p = 5$ mm. The tool was made of hardened W302-H13 mild steel which is often used to Friction Stir weld Aluminium alloys [51]. The design of the tool excluded tool threading in order to provide a good validation of the thermal model.

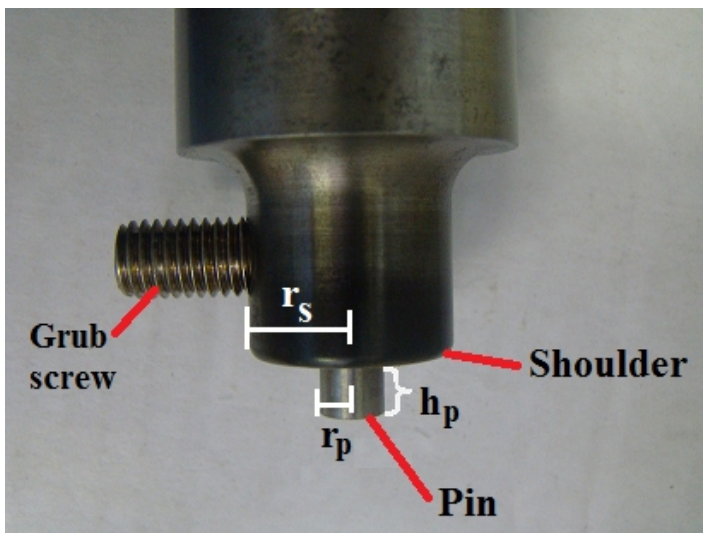

Figure 4-3: Friction Stir Welding tool used in Aluminium welding

4.4.2 Backing Plate and Clamping Mechanism

For the Aluminium welding, the backing plate material was W302-H13 mild steel which matched the clamping material. The backing plate was fitted into the already machined slot of the I-STIR PDS platform before the workpiece was placed on top. After the backing plate was put in

place, the workpiece plates needed to be clamped with the weld centre line on the rigid backing plate in a manner that would prevent the plates from separating at the join line during the weld [10].

Figure (4-4) shows how the Aluminium plates were clamped onto the backing plate by means of clamping bars and clamps all machined out of mild steel. The clamping bars on top of the workpiece were placed 60mm from the weld line on both the advancing and retreating sides. The dimensions of the steel clamping region in contact with the aluminium on the top surface of the workpiece is 407 mm × 13 mm. The position of the clamping was restricted to allow for the passing of the tool and the positioned thermocouples.

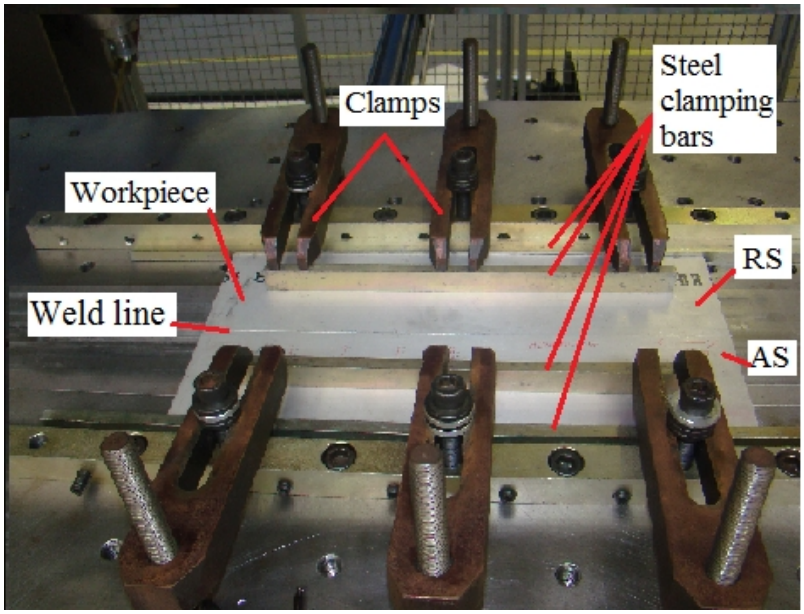

Figure 4-4: Aluminium Workpiece and Clamping

4.4.3 Thermocouple positions

The layout of the thermocouple positions was taken from the work by Frigaard and co-workers [12] for the Aluminium FSW. The positions of the thermocouples in the workpiece as seen from

the top of the advancing side (AS) is shown in an unscaled diagram, Figure (4-5).

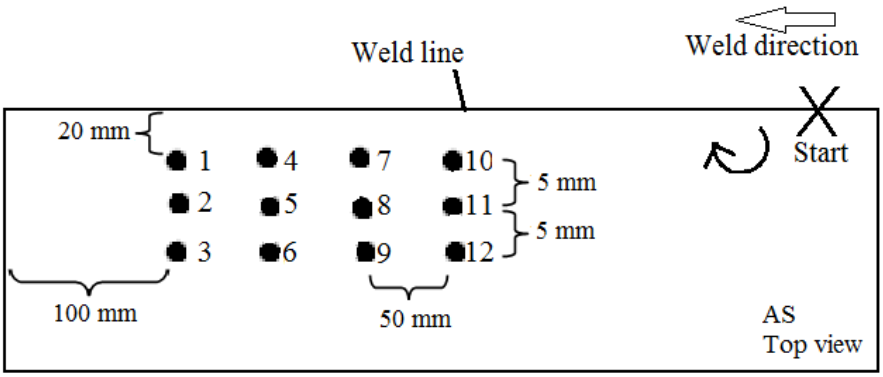

Figure 4-5: Thermocouple positions in Aluminium plates

The first row of thermocouples (1, 4, 7 and 10) were placed at 20 mm to the weld line. The rows of thermocouples were separated by 5 mm and the columns were separated by 50 mm. The first column of thermocouples (1, 2 and 3) were placed at 100 mm from the edge of the plate.

4.4.4 Welding Parameters

Parameters for the welding of Aluminium Al 6082-T6 were chosen from the work of Oyedemi [52]. Table (4.1) summarizes the different operating input parameters chosen to make the Aluminium welds.

Rotational Speed (rad/min)	**Feedrate (mm/min)**	**Shoulder Plunge Depth (mm)**	**Tool Tilt**	**Dwell Time (s)**	**Weld Length (mm)**
400	120	0.2	2°	20	400
600	120	0.2	2°	20	400
600	240	0.2	2°	20	400
600	360	0.2	2°	20	400
800	120	0.2	2°	20	400

Table 4.1: Welding parameters used for Al 6082-T6 welds

4.5 Titanium Ti 6Al-4V welds

4.5.1 The Friction Stir Welding Tool

The tool used to weld the 3 ±0.2 mm thick Titanium Ti-6Al-4V plates, shown in Figure (4-6), had a flat shoulder of a radius $r_s = 7$ mm and a conical pin with a 4 mm radius at the shoulder (r_t) and a 2 mm radius at the end of the pin (r_b). A conical shaped pin was used because it has been proven to produce defect free welds [4]. The tool material used was Lanthanated Tungsten, WL10. This material is suitable to weld Titanium because it can withstand high temperatures (1100 - 1200 ^{o}C) and is inert to Titanium. Mashinini [4] found that minimal wear was identified, and the tool material maintained its mechanical properties during the welding

of Ti-6Al-4V.

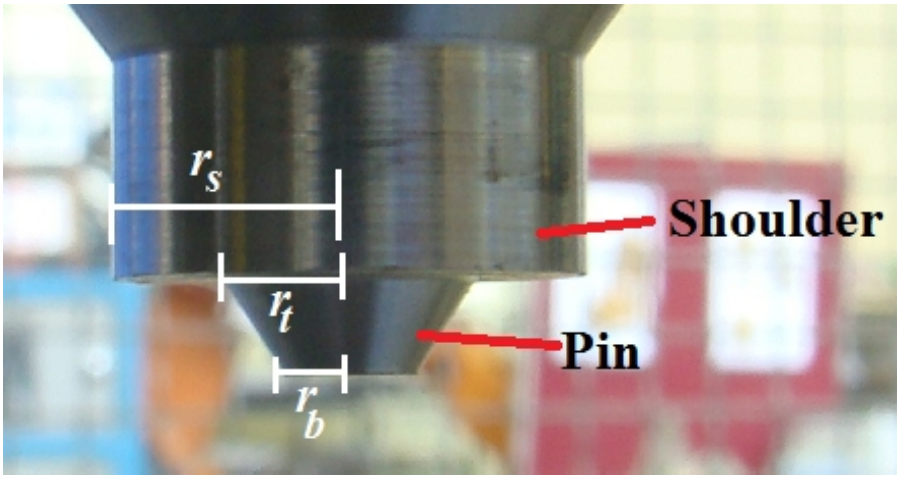

Figure 4-6: Tool shoulder and pin used in Titanium welding

When welding with high melting point materials such as Titanium, it is important to protect the workpiece and the tool from oxidation [4] using a shielding mechanism. Inert Argon was used as a shielding gas. This was injected into the area around the tool and the weld through the tool holder.

4.5.2 Backing Plate and Clamping Mechanism

For the higher temperature welding of Titanium, a backing plate insert of Haynes 230 alloy into EN 10025 steel was selected because it can be used continuously at temperatures up to 1150°C and allows very little heat to escape from the workpiece. Similarly to the method used to weld the Aluminium plates, the backing plate was fitted into the already machined slot of the I-STIR PDS platform before the workpiece was placed on top. After the backing plate was put in place, the workpiece plates needed to be clamped. Since the Titanium sheets were thinner than the Aluminium sheets, the clamping bars needed to be clamped closer to the weld line to

prevent the plates from lifting at the weld line. Mild steel clamping bars and clamps were used for this purpose (see Figure (4-7). The clamping bars were placed at 35 mm away from the weld line on both sides of the weld and covered 300 mm × 185 mm of the Ti 6Al-4V surface.

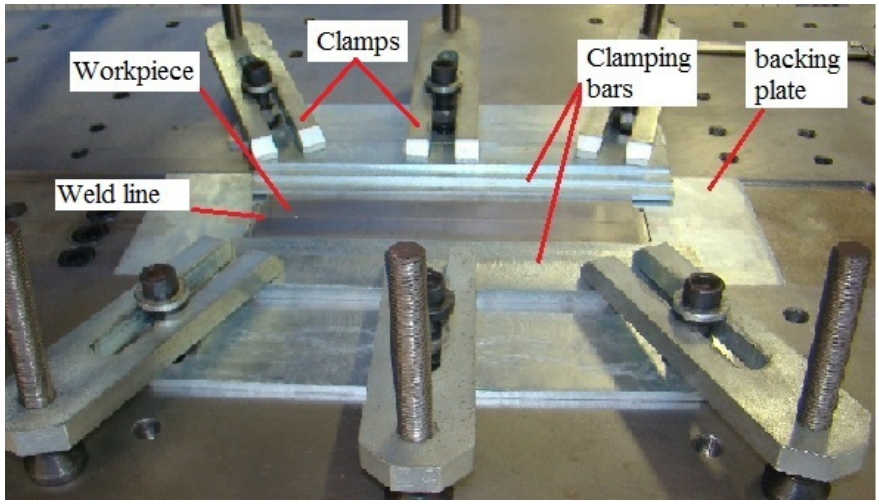

Figure 4-7: Titanium workpiece and clamping

4.5.3 Thermocouple positions

The layout of the thermocouple positions was taken from the work by Mishra [33] for the Titanium Ti 6Al-4V welds. Figure (4-8) shows the unscaled diagram of the advancing side (AS) plate as viewed from the top. The tool used for the welding of Titanium had a smaller shoulder radius than that of the tool used to weld Aluminium. For this reason, the thermocouples used in the Titanium welding could be placed closer to the weld line than in the Aluminium welding.

Since the thermal conductivity of Ti 6Al-4V (± 20 W/m·K) is much lower than the thermal conductivity of Al 6082-T6 (± 180 W/m·K), it would also be desirable to place the thermocouples closer to the tool and to each other since the heat dispersed from the centre of the weld

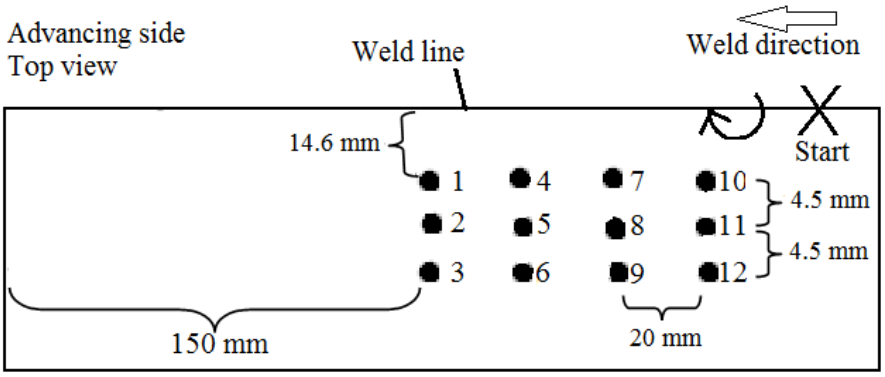

Figure 4-8: Thermocouple positions in Titanium plates

travels less distance in the Titanium than the heat in the Aluminium for the same amount of time.

4.5.4 Welding Parameters

Parameters for the welding of Titanium Ti 6Al-4V were selected from the work of Mashinini [4]. Table (4.2) shows the operating input parameters chosen to make the Titanium Ti 6Al-4V Friction Stir weld. Only one weld was performed on Ti 6Al-4V since it was the intention to investigate whether the heat transfer model of Aluminium could be readily adapted to the FSW of Ti 6Al-4V and not to provide a full validation of the model.

Rotational Speed (rad/min)	450
Feed rate (mm/min)	55
Shoulder Plunge Depth (mm)	0.1
Tool Tilt (^{o})	0.5
Dwell Time (s)	2
Weld Length (mm)	200

Table 4.2: Welding parameters used for Ti 6Al-4V weld

Chapter 5

Results and Discussion

5.1 Introduction

In this chapter the experimental and numerical results from the Aluminium Al 6082-T6 and Titanium Ti 6Al-4V welds will be presented and discussed. In order to validate the model, the numerical results for both Aluminium and Titanium will be compared with the experimental results either obtained in this study or with those obtained by other researchers [33, 35, 53, 54]. The numerical results will be presented for both Aluminium and Titanium as follows:

- 2D plots of the predicted temperature in the workpiece,
- Predicted temperatures at specific locations on the tool surface, and
- Predicted temperatures at different thermocouple locations.

Since the model assumes a stationary tool with a moving workpiece which is contrary to the actual FSW, the temperature-position curves for the experimental and numerical results

needs to be obtained in different ways. Experimental temperatures at a given thermocouple represent the thermal history during the welding. These temporal values can then be converted into tool position since the feed rate is known resulting in the temperature-position curve for given thermocouple. In the model, since the workpiece is moving, the temperature-position curves can be obtained by reading values on any line drawn parallel to the motion of the tool. Three lines were used for the comparisons where the first line closest to the weld line connects thermocouple positions 1, 4, 7 and 10, the second line connects 2, 5, 8 and 11 and the third line connects 3, 6, 9 and 12 (see Figures (4-5) and (4-8)). The three temperature-position curves associated with these three lines in the model correspond to the experimentally obtained temperature-position curves for thermocouple 10, 11 and 12 for Aluminium and 1, 2 and 3 for Titanium respectively. The temperature-position curves were shifted until the maximum experimental and numerical temperatures coincided.

A parametric study on the Aluminium model was also performed to determine the influence of rotational speed and feed rate on the maximum temperatures reached at locations on the tool surface.

In order to determine how accurately the model predicts the temperatures in the workpiece, the outcomes of an error analysis will be discussed. Since there is no standard used by other researchers to determine the accuracy of a model, temperature predictions of this study are considered to be in good agreement with experimental results if the relative percentage error involved is less than or equal to 15%. This value was chosen since it lies within the percentage error ranges found by other researchers [33, 24, 55, 12]. Furthermore, 15% of the melting of point of either Al 6082-T6 or Ti 6Al-4V is relatively small in comparison to the respective melting points (± 555 ^{o}C for Al 6082-T6 and ± 1600 ^{o}C for Ti 6Al-4V).

5.2 Results and Discussion for Aluminium Al 6082-T6

5.2.1 Surface and Isosurface Plots

Figure (5-1) shows the predicted workpiece temperatures for a rotational speed of 600 rpm and a feed rate of 360 mm/min where the value, 405.2 °C, shown on the plot, is the maximum predicted temperature for the workpiece at these welding conditions and is located at the top of the tool pin at the point T_{max} shown in Figure (5-2). This temperature is approximately 73% of the melting point of Aluminium (±555 °C). This temperature cannot directly be compared with experimental results obtained in this study since the thermocouples were placed 20 mm from the weld line and Al 6082-T6 data is limited. This temperature was however found to be in agreement with results discussed in a review on FSW [33] where the maximum temperatures during the FSW of 6.35 mm Al 7075-T651 plates were found to be between 400 to 480 °C.

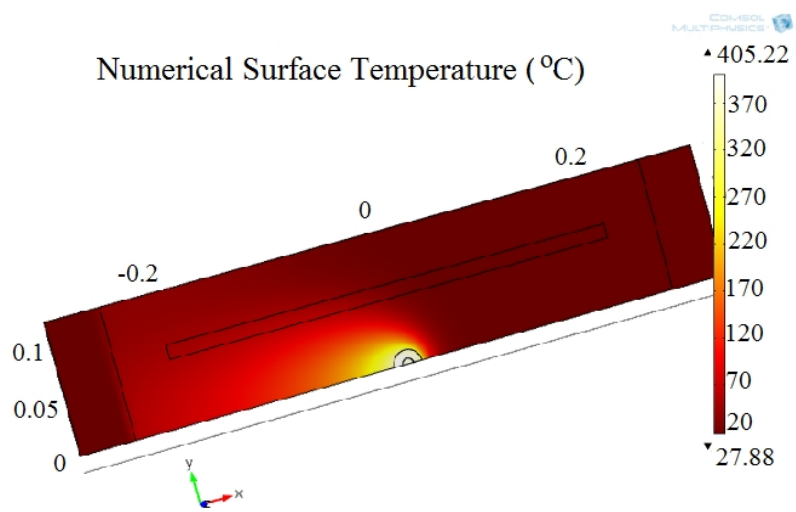

Figure 5-1: Numerical temperature surface plot for Aluminium: Rotational speed of 600rpm and feed rate of 360 mm/min

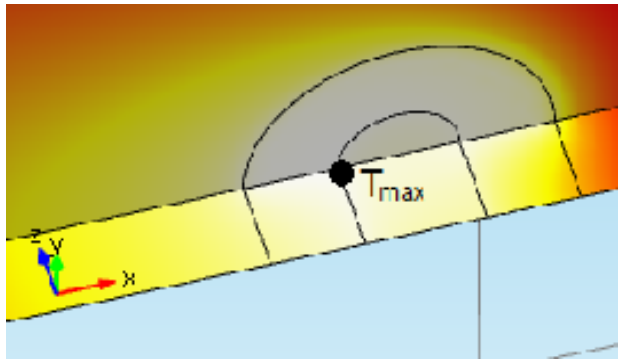

Figure 5-2: Position of maximum workpiece temperature

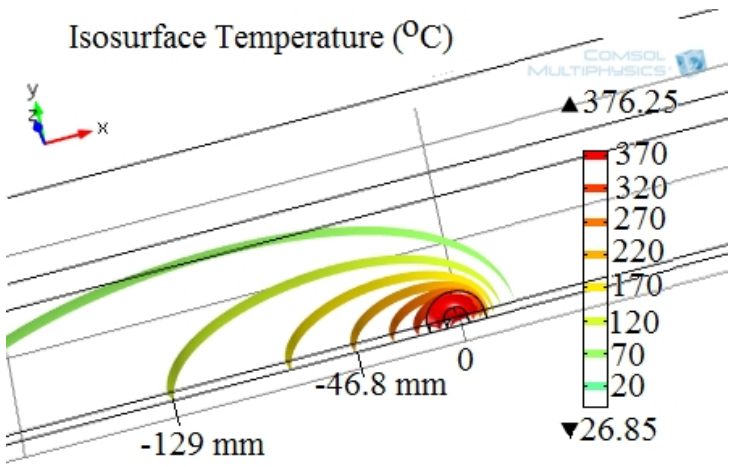

Figure 5-3: Temperatures along isosurfaces near the tool for Aluminium

The isosurface plot for the predicted temperatures for Aluminium for the rotational speed of 600 rpm and the feed rate of 360 mm/min is shown in Figure (5-3). From Figures (5-1) and (5-3) the flow of heat around and in the wake of the tool can clearly be seen. The temperatures higher than 220 °C are concentrated within a 50 mm radius of the tool. At monitoring points at 18 mm and 28 mm from the center of the tool in the y-direction, the temperature difference was found to be approximately 90 °C whereas the temperature difference between points 38

mm and 48 mm away from the tool is only about 30 ^{o}C. Outside of the 30 mm radius of the tool, large regions correspond to the same isotherms (70 ^{o}C and 90 ^{o}C) implying that points in these regions all have very little temperature difference between them ($\pm$2 to 5 ^{o}C). These small temperature differences could be due to the high thermal conductivity of Aluminium which contributes to thermal homogeneity in the material [35] since the heat dissipates quickly and evenly throughout the material.

5.2.2 Model Validation

Experimental temperature readings, taken from the data collected at positions 10, 11 and 12 (see Figure (4-5)), were compared to the predicted values at the same position in the model. The first set of results, see Figure (5-4), shows the temperature readings at thermocouple 10 and the corresponding numerically predicted values for three different rotational speeds at a constant feed rate of 120 mm/min, Figure (5-5) shows the numerical and experimental results obtained for a constant rotational speed of 600 rpm and three different feed rates, while Figure (5-6) shows temperature-position curves for the thermocouples at positions 10, 11 and 12 (see Figure (4-5)) for the rotational speed of 600 rpm and the feed rate of 360 mm/min.

From Figures (5-4) and (5-5) it can be seen that the model gives a good prediction of the experimental results since the numerical temperature-position curve almost matches that of the experimental results but it is interesting to notice that the accuracy of the model increases with higher feed rates. The most accurate estimate was found to be the estimations for the 600 rpm and 360 mm/min weld. The results for thermocouples 10, 11 and 12 at these welding conditions are shown in Figure (5-6) where the most accurate prediction occurs at position 11 for both the maximum temperature and the overall temperature trend. Interestingly enough, the tem-

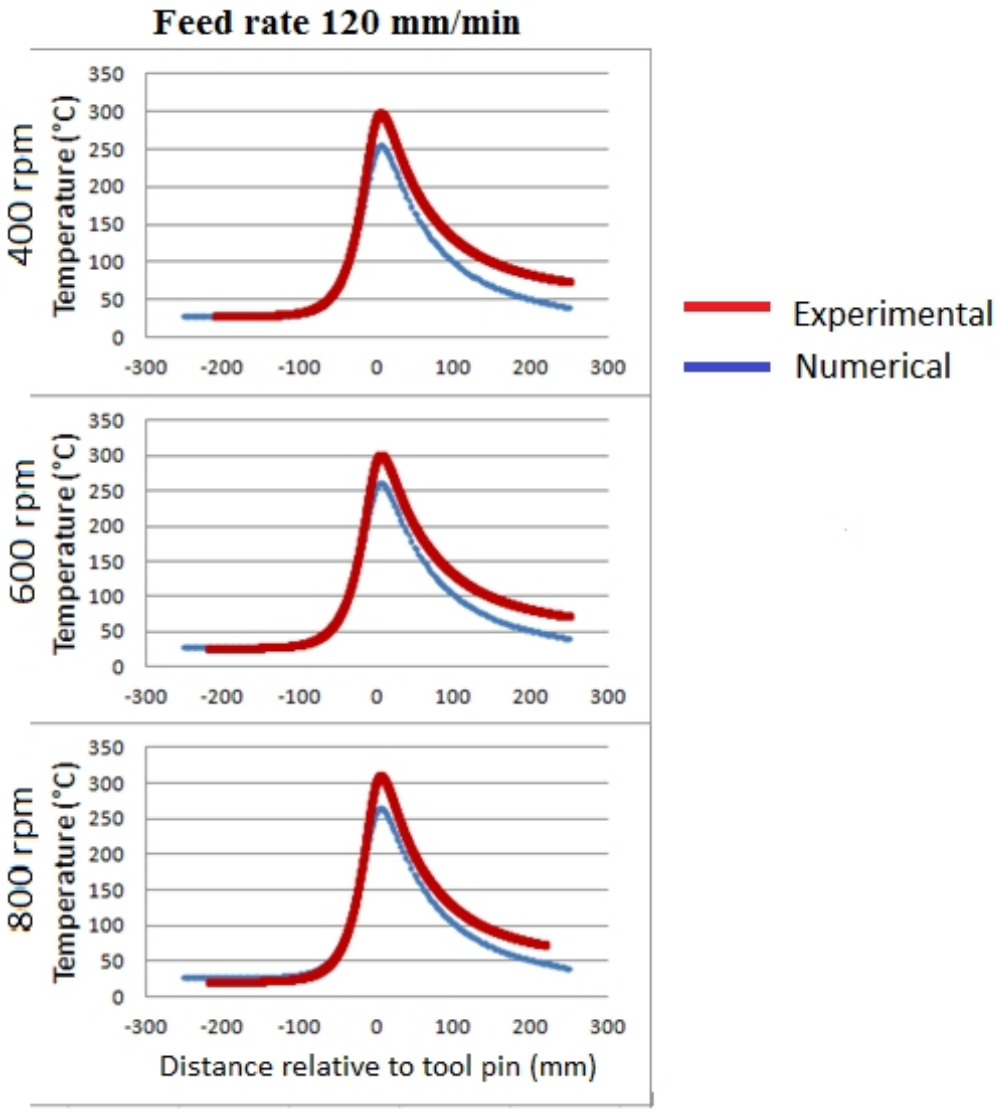

Figure 5-4: Temperature for Aluminium: feed rate of 120 mm/min, 20 mm from weld line

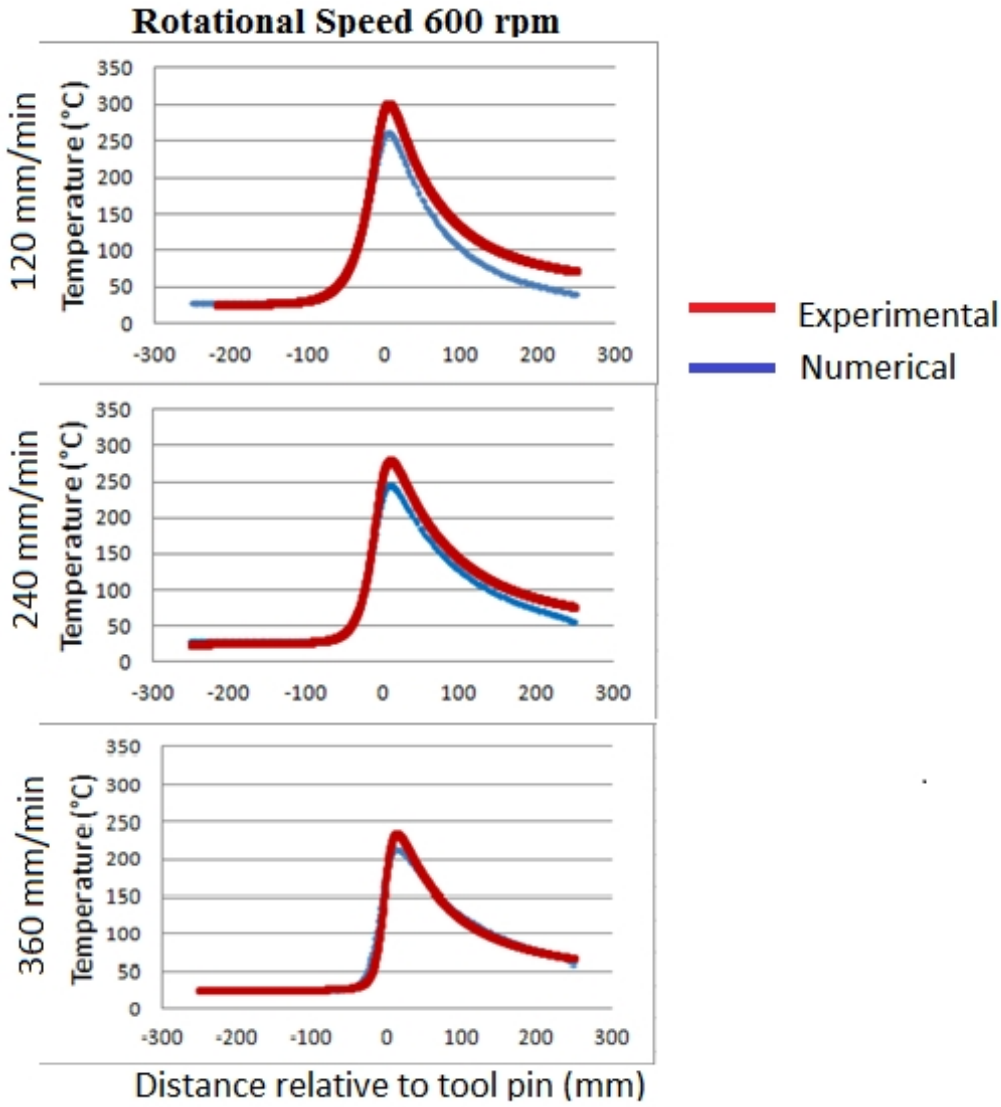

Figure 5-5: Temperature for Aluminium: rotational speed of 600 rpm, 20 mm from weld line

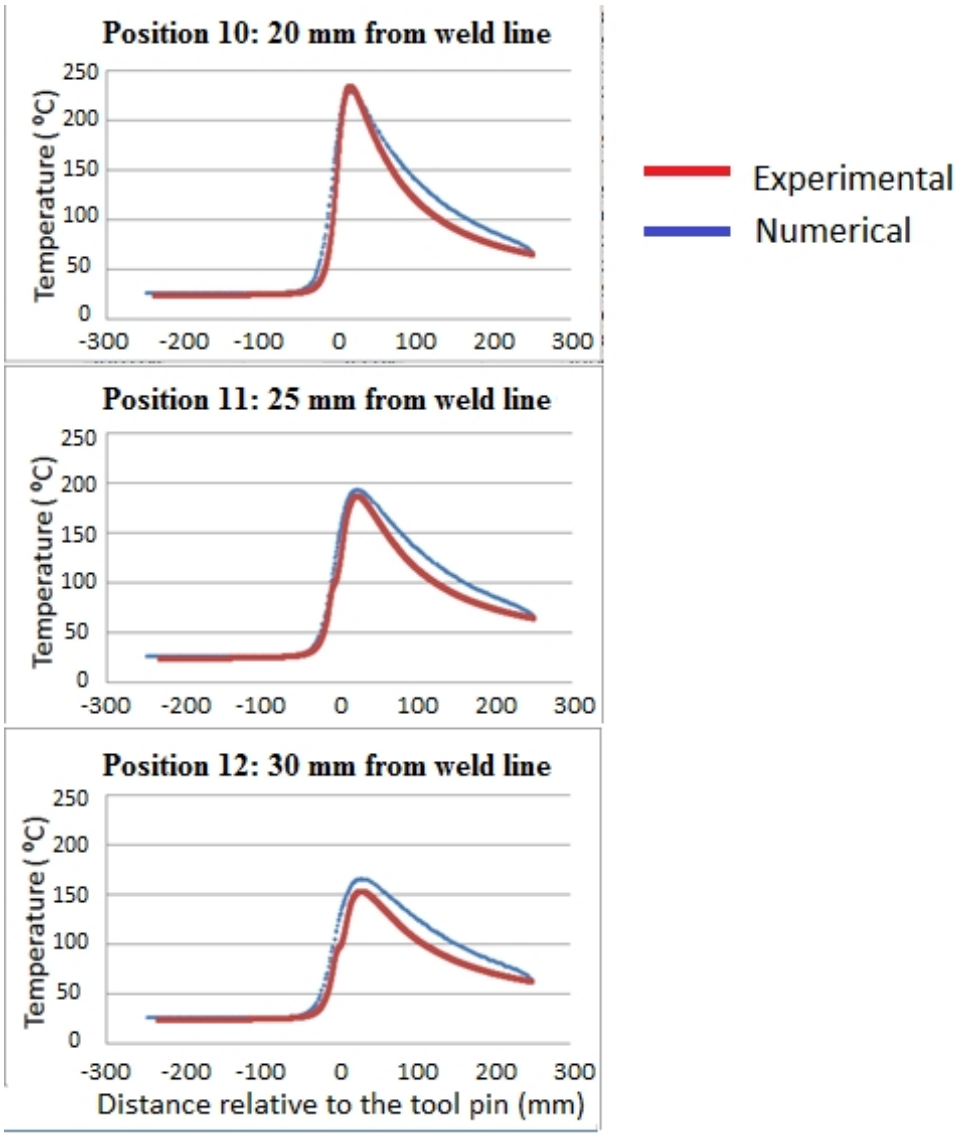

Figure 5-6: Temperatures for Aliminium for 600 rpm and 360 mm/min at 20 mm, 25 mm and 30 mm from weld line

perature was over estimated for positions further away from the weld line and underestimated near the weld line. The reason for this is unknown but a possible reason could be due to the thermal conductivity for the material which is specific to AA 6061-T6 and not for Al 6082-T6.

Figures (5-7) and (5-8) display the maximum experimental and numerical temperatures at a constant feed rate of 120 mm/min and for a constant rotational speed of 600 rpm.

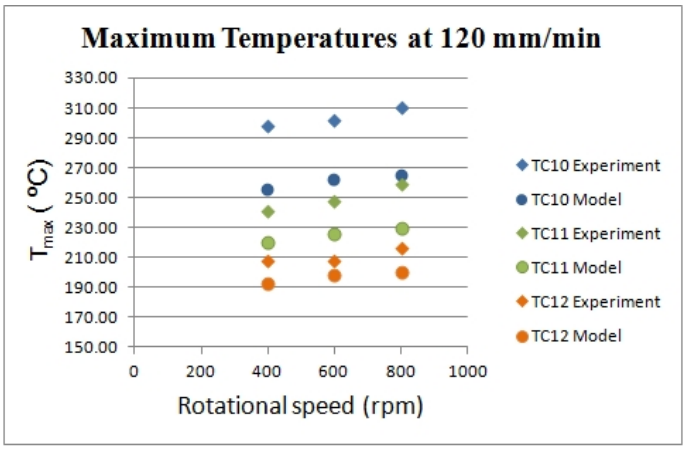

Figure 5-7: Maximum temperatures at constant feed rate for Aluminium

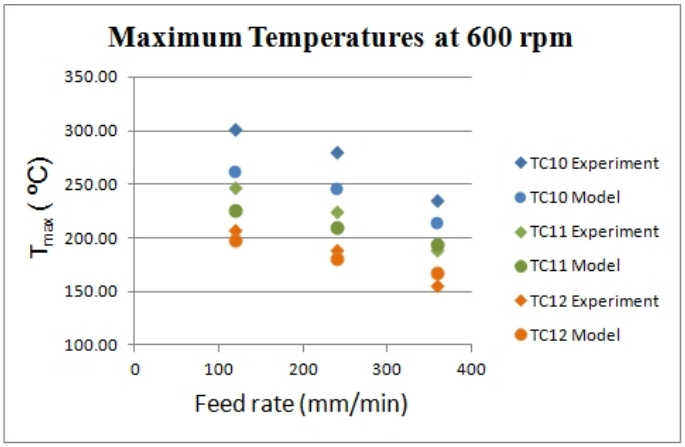

Figure 5-8: Maximum temperatures for constant rotational speed for Aluminium

The maximum experimental temperatures measured at the thermocouple closest to the tool (20 mm from weld line), for the Aluminium welds, were between 42% and 56% of the melting point of Aluminium Al 6082-T6 for feed rates of between 120 and 360 mm/min respectively. The numerical prediction for the maximum temperatures at the same thermocouple position ranges between 34% and 47.8% of the melting point. These numerical results, although lower than the experimental results (±20 °C), are still comparable with results found by Mishra [33] who recorded temperatures of approximately 250 °C at positions 10 to 20 mm away from the tool for 6.35 mm thick Al 7075-T671 plates.

The following trends in the maximum temperatures are apparent in both the numerical and experimental results shown in Figures (5-7) and (5-8) and are in agreement with other researchers [35, 53]:

- Temperature decreases with increasing feed rate, and
- Temperature increases with increasing rotational speed.

The temperature decreases with increasing feed rate since exposure time is lessened with increasing feed rate. The fact that the temperature increases with increasing rotational speed is expected in the model since the heat flux boundary condition is directly dependent on the rotational speed (see Equation (3.8)). This trend is also expected in the experimental results since at high rotational speeds, the relative velocity between the tool and the workpiece is higher which causes the heat generation to increase and hence temperatures to increase.

The following trends are evident in the comparison between the numerical and experimental results:

- The predicted temperatures are lower than the experimental temperatures for most welding conditions.
- For a rotational speed of 600 rpm, the model tends to over estimate the experimental temperature when the feed rate and distance from the weld line is increased, and
- The feed rate appears to have a larger effect on the workpiece temperature than the rotational speed.

There are some possible explanations why the estimated maximum temperatures are lower than the experimental results, namely:

- The numerical model does not account for all the heat being transferred into the workpiece which could have arisen from the choice of heat flux at the tool shoulder and pin boundaries, and
- The temperature dependent function for the thermal conductivity of the material is specific to AA 6061-T6 since this data is not available for Al 6082-T6. This conductivity

could possibly allow for the heat to be dissipated too much throughout the workpiece.

5.2.3 Error Analysis

It is important to determine how accurately the model predicts the maximum temperature and the overall trend of the temperature curve. For any value, p, that is approximated by another value, p_i, the relative percentage error involved in the approximation is given by the following:

$$e = \frac{|p - p_i|}{p} \times 100\% \tag{5.1}$$

Using Equation (5.1), the error involved in predicting the maximum temperature at a specific thermocouple position, can be calculated using the following formula:

$$e^{\max} = \frac{\left| T^{\max}_{\mathrm{experiment}} - T^{\max}_{\mathrm{model}} \right|}{T^{\max}_{\mathrm{experiment}}} \times 100\% \tag{5.2}$$

where $T^{\max}_{\mathrm{experiment}}$ is the maximum temperature measured experimentally and $T^{\max}_{\mathrm{model}}$ is the maximum predicted temperature for a specific thermocouple position.

In order to calculate the error involved in predicting the overall temperature curve, the area under the curve was chosen as a possible means of comparison. The area under the curve was calculated using the Trapezoidal rule.

The relative error for the area under the curve is calculated using the following formula:

$$e^{\mathrm{area}} = \frac{|A_{\mathrm{exp}} - A_{\mathrm{model}}|}{A_{\mathrm{exp}}} \times 100\% \tag{5.3}$$

where e^{area} is the relative error of the area under the curve, A_{exp} is the area under the experimental temperature-position curve and A_{model} is the area under the estimated temperature-position curve.

For each of the 5 welds (see temperature-position curves in Figures (5-4) and (5-5)), the following relative errors were calculated for the maximum temperature and the area under the curve at the given thermocouple positions:

Rpm	**Feed rate (mm/min)**	$\mathbf{e}^{\text{max}}_{\text{TC10}}$	$\mathbf{e}^{\text{max}}_{\text{TC11}}$	$\mathbf{e}^{\text{max}}_{\mathbf{TC12}}$	$\mathbf{e}^{\text{area}}_{\mathbf{TC10}}$
400	120	14.5%	8.7%	7.0%	23.4%
600	120	13.2%	8.6%	4.6%	17.7%
800	120	14.6%	11.6%	7.4%	11.7%
600	240	12.2%	6.7%	3.6%	10.2%
600	360	9.0%	3.2%	7.8%	15.5%

Table 5.1: Relative error in temperature prediction for Aluminium

These values suggest that the model gives a generally good prediction of the maximum temperatures since the error on average is only 8.8%. The average relative error involved in predicting the overall temperature trend at a point is 15.7% which slightly higher than the desired value but still reasonable. The largest error in the maximum temperature prediction of 14.6% occurs at the highest rotational speed, 800 rpm which equates to a 45.2 ^{o}C difference between the maximum experimental temperature and the predicted temperature at the position of thermocouple 10. This difference between numerical and experimental temperature is similar to those obtained by other researchers [24, 55] for Aluminium alloys. The model most accurately

predicts the maximum temperature at the highest feed rate of 360 mm/min at the position of thermocouple 11 with a 3.2% error which equates to a 6.0 °C difference. The error for the area under the curve tends to decrease with increasing rotational speed. In summary the accumulated errors can provide some useful information about the accuracy of the model. From the table it is clear that the model is better at predicting the maximum temperatures at a certain point than it is at predicting the overall temperature trend since on average, $\mathbf{e}^{\text{max}}_{\text{TC10}} < \mathbf{e}^{\text{area}}_{\mathbf{TC10}}$.

5.2.4 Contour Plots for All Twelve Thermocouples

Until now, focus has been on the comparisons of the predicted and experimental temperatures at thermocouples 10, 11 and 12. In order to determine the how well the model is able to predict the experimental temperatures as a whole, temperature values for all twelve thermocouples for both the experimental and numerical results have been represented in the form of contour plots.

The model predicts the steady-state temperatures of the workpiece for the instant in time when thermocouple 10 has its maximum value. The experimental temperatures for the twelve positions were hence selected for the same instant in time.

Figures (5-9) and (5-10) show the contour plots for the temperatures at the thermocouple positions where the y-axis represents the distance from the weld line and the x-axis represents the distance from the left side of the workpiece when Figure (5-1) is used as a reference. Table (5.2) shows the (x, y) co-ordinates in mm relative to the contour plots and the corresponding temperature in °C as well as the calculated error between the experimental and the numerical results. The error was calculated using Equation (5.1). The plots were generated by interpolating the temperatures between the values obtained at the thermocouple positions. The experimental data was obtained for the instant in time when thermocouple 10 reached its

maximum value.

	1	**2**	**3**	**4**	**5**	**6**	**7**	**8**	**9**	**10**	**11**	**12**
x (mm)	400	400	400	350	350	350	300	300	300	250	250	250
y (mm)	20	25	30	20	25	30	20	25	30	20	25	30
$\mathbf{T}_{\text{model}}$ (^{o}C)	27.9	27.9	27.9	27.9	27.9	27.9	30.6	30.2	29.9	208.3	162.1	127.8
$\mathbf{T}_{\text{exp}}$ (^{o}C)	23.7	23.7	23.8	24.3	24.3	24.5	41.2	42.2	43.1	235.6	182.2	144.6
e	**17.7**	**17.7**	**17.2**	**14.8**	**14.8**	**13.9**	**25.7**	**28.4**	**30.6**	**11.6**	**11.0**	**11.6**

Table 5.2: Errors for temperatures at thermocouple co-ordinates for Aluminium

The results from the contour plots appear to be in good agreement since the corresponding isosurfaces in the numerical and experimental plots are only a few millimeters apart. The error values for most of the positions are close to 15% which suggests that the model predicts the temperature trend at the twelve thermocouples well, although the temperatures are slightly lower than the experimental results. The largest errors occur at positions 7,8 and 9. If we compare the contour plots at the $x = 300$ mm line where these thermocouples are located, it can be noted that in the numerical results, the 60 ^{o}C isosurface has not reached this line yet. In the experimental results, however the 60 ^{o}C isosurface has already reached the $x = 300$ mm line. This discrepancy could be due to the thermal conductivity value in the model which is not specific to Al 6082-T6.

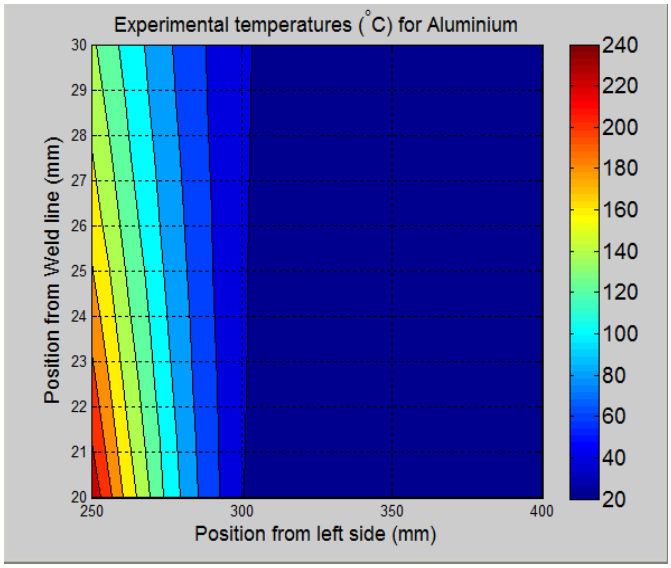

Figure 5-9: Contour plot for experimental thermocouple readings for Aluminium

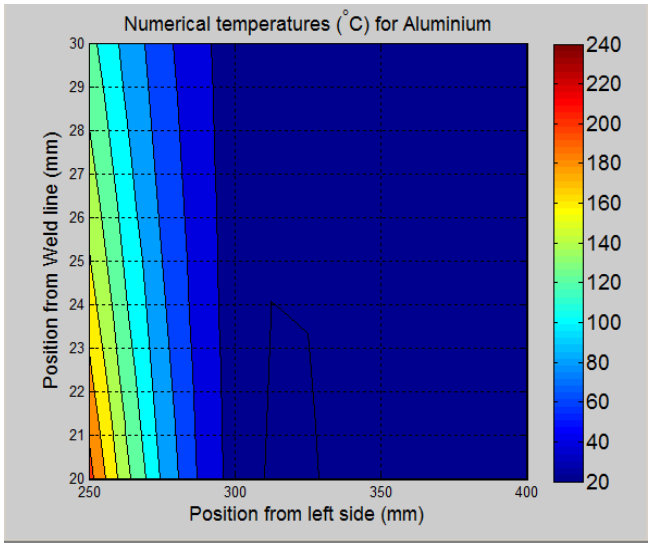

Figure 5-10: Numerical contour plot for thermocouple positions for Aluminium

5.2.5 Parametric Study

To investigate the temperatures in the vicinity of the tool surface, three points in the numerical domain were selected for observation. Figure (5-11) shows the positions of the three points, A (at the tool shoulder edge), B (at the top of the pin) and C (at the bottom of the pin) where the predicted temperatures were obtained for the Aluminium welds. Results for the positions are tabulated in Table (5.3). Equivalent experimental temperatures are not available as it was not possible to place thermocouples so close to the tool pin for fear of damage.

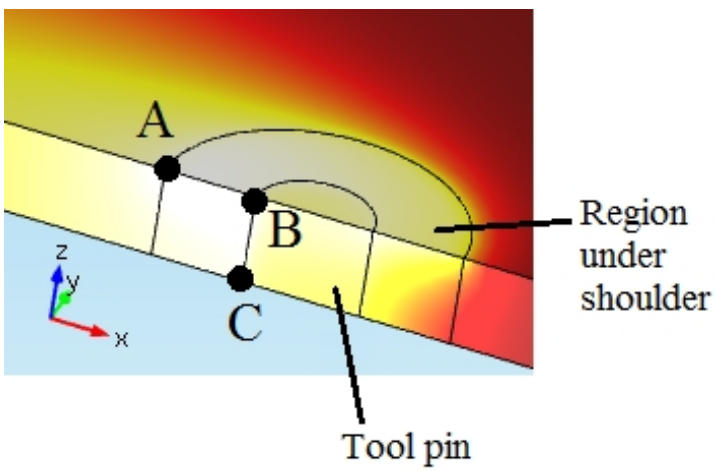

Figure 5-11: Tool surface positions for Aluminium

Rotational Speed (rpm)	**Feed rate (mm/min)**	$\mathbf{T}_A$ **(°C)**	$\mathbf{T_B}$ **(°C)**	$\mathbf{T_C}$ **(°C)**
400	120	383.6	370.7	400.9
600	120	379.7	392.0	406.0
800	120	384.8	408.3	396.4
600	240	383.4	405.9	392.3
600	360	385.5	405.2	391.2

Table 5.3: Predicted tool temperatures for Aluminium

The highest temperature for the given welding conditions was predicted to be 408.3 °C which was found at position B, the top of the tool pin. This value corresponds to the rotational speed of 800 rpm and the feed rate of 120 mm/min. Experimental validation could not be done for these temperatures since thermocouples were placed too far away from the tool. From the table the temperature trends are not very clear. At all three positions, the temperatures do not decrease with increasing feed rate as found in the regions further away from the tool. A possible reason for this deviation from the expected trend could again come from the specific heat and conductivity values which are specific to a different Aluminium alloy. It could also be that the shear stress function in the flux term is not as accurate for the high temperatures near the tool.

In order to further study any trends in the temperatures at the three points, A, B and C, a parametric study was undertaken for a broader range of welding conditions that was not included in the experimental study. This parametric study was performed for the feed rates ranging from 100 to 1000 mm/min and the rotational speeds ranging from 300 to 1200 rpm.

The results for the parametric studies performed for each of the points A, B and C are depicted by means of two plots, each representing the same data in different ways. The two different plots aid in the interpretation of the results. Figures (5-12) and (5-13) show the results for point A, Figures (5-14) and (5-15) show the results for point B and Figures (5-16) and (5-17) show the results for point C.

From these parametric studies, the trends in the predicted temperatures at the three tool surface points are clearer than in the limited values provided in Table (5.3). From Figures (5-12), (5-14) and (5-16), the following trends are clear. The temperatures at position B and C on the tool surface increase with increasing rotational speed and decreasing feed rate which is the expected trend as mentioned before. There is, however, a change in predicted temperature behaviour for position A at the edge of the shoulder where the highest feed rate yields the highest temperatures. This could be an anomaly in the model or there could be excess frictional heating at the edge of the shoulder. Further experimental temperature measurements are required to verify this.

From Figures (5-13), (5-15) and (5-17), the effect of the rotational speed on the temperature is more noticeable. For each of the three points, the rotational speeds from 840 to 1200 rpm tend to have a smaller effect on the maximum temperature of the workpiece than the lower rotational speeds such as 300 to 660 rpm. This effect is most noticeable at point A since there is a 30 ^{o}C increase from 300 rpm to 660 rpm while there is only a 10 ^{o}C increase from 660 rpm to 1200 rpm. A similar trend was recorded for 6.4 mm Al 6061 T6 plates that were FS welded at 120 mm/min [33] where a 40 ^{o}C increase was observed from 300 rpm to 650 rpm and only 20 ^{o}C increase from 650 rpm to 1000 rpm. Since rotational speeds greater than 650 rpm

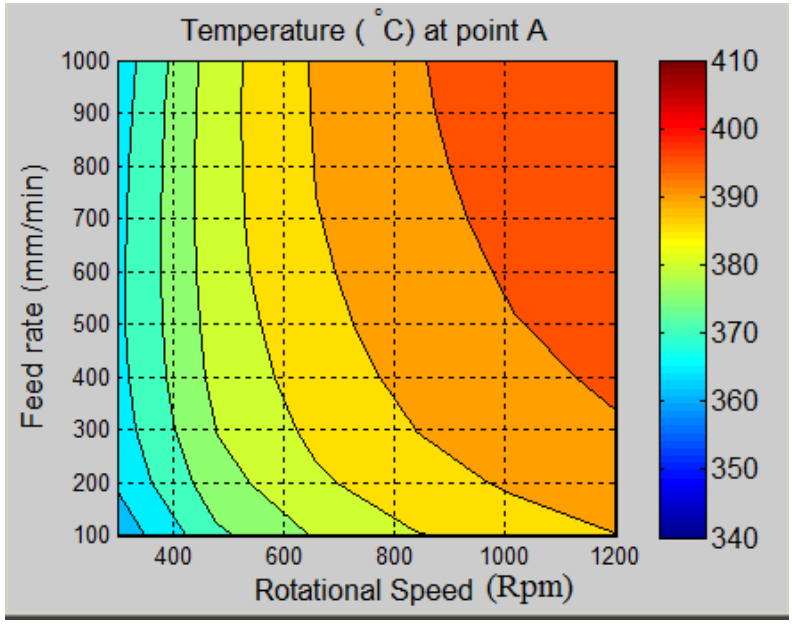

Figure 5-12: Predicted temperature at position A for various parameters plot 1

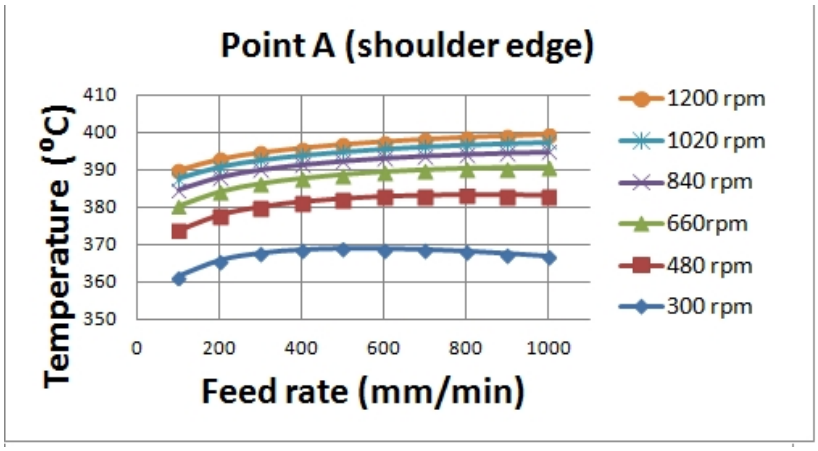

Figure 5-13: Predicted temperature at position A for various parameters plot 2

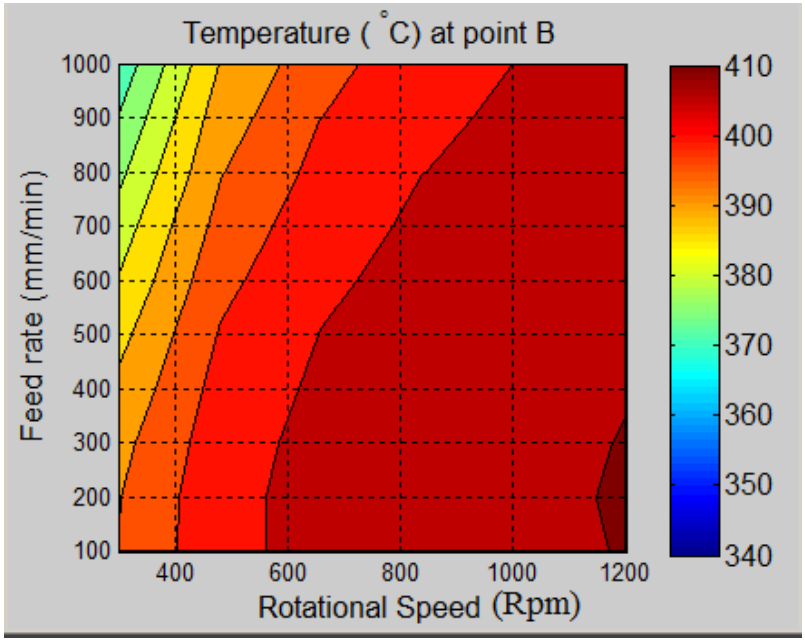

Figure 5-14: Predicted temperature at position B for various parameters plot 1

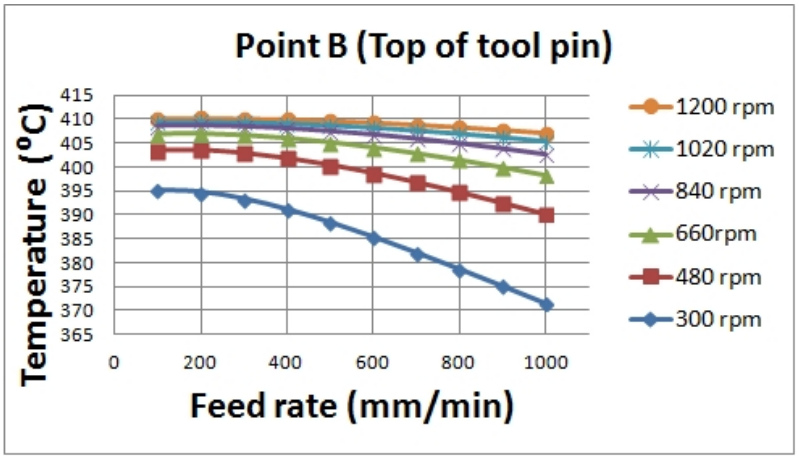

Figure 5-15: Predicted temperature at position B for various parameters plot 2

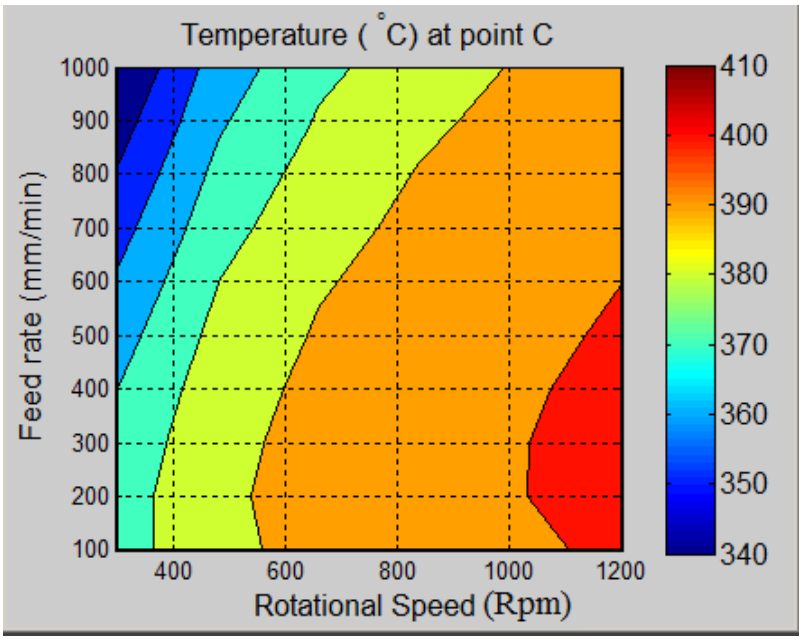

Figure 5-16: Predicted temperature at position C for various parameters plot 1

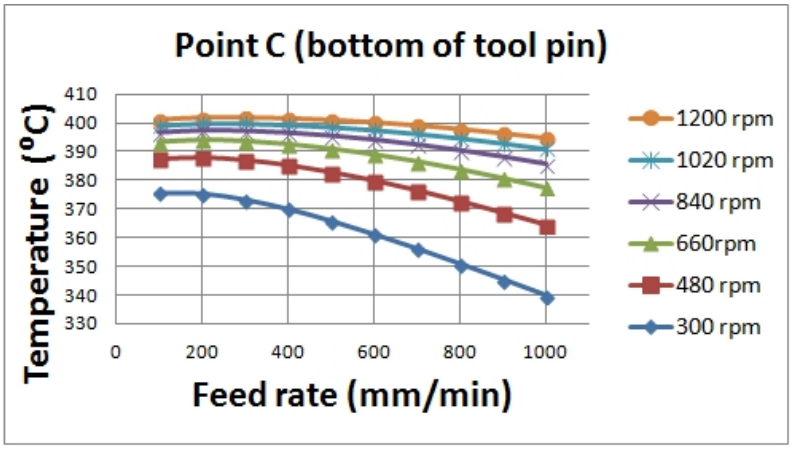

Figure 5-17: Predicted temperature at position C for various parameters plot 2

yield temperatures greater than 380 ^{o}C, the shear stress of the material at these temperatures, is very low in the order of ±20 MPa (see Figure (3-1)). This could be a reason for the small temperature changes at higher rotational speeds since the shear stress has a direct influence on the heat flux. It appears from this trend that the maximum temperature of the Al 6082-T6 workpiece tends towards an upper limit of approximately 410 ^{o}C (73.87% of the melting point) and increasing the rotational speed more than 1200 rpm would not have a big effect on the maximum temperature of the weld.

It appears from Figures (5-13), (5-15) and (5-17), that the rotational speed has a more noticeable effect on the temperature than the feed rate since in all the plots for the parametric studies, the change in temperature for the various feed rates is only up to ±30 ^{o}C while the rotational speed changes yield temperature changes of up to ±50 ^{o}C. Further experimental data is required to verify this.

It can also be deduced that the temperatures at the tool pin surface (points B and C) are generally higher than the temperatures found at the shoulder edge (at A) with the highest temperatures occurring at the top of the pin. This could be due to the accumulative heat flux from the tool shoulder and pin at these points.

The predicted temperature (± 405 ^{o}C) at point B that corresponds to 1200 rpm and 480 mm/min lies within a range of experimental results obtained by Frigaard and co-workers [12] who obtained temperatures of between 370 ^{o}C and 480 ^{o}C from thermocouples at ±6 mm away from the weld line for 6 mm Al 6082-T6 plates at 1500 rpm and 480 mm/min. Although the predicted temperatures are lower than most of the experimental results, this is expected since the rotational speed was lower in the model used in this study. This comparison does assist to show that the model does indeed give a reasonable prediction of the temperatures involved in

the FSW of Al 6082-T6.

5.3 Results and Discussion for Titanium Ti 6Al-4V

5.3.1 Surface and Isosurface Plots

Only one Titanium Ti 6AL-4V weld was performed because of time and cost constraints. For this weld, the rotational speed of 450 rpm and a feed rate of 55 mm/min was used.

In Figure (5-18), the numerical estimation for the surface temperature of the Titanium workpiece is shown. The predicted isosurface temperature plot is shown in Figure (5-19).

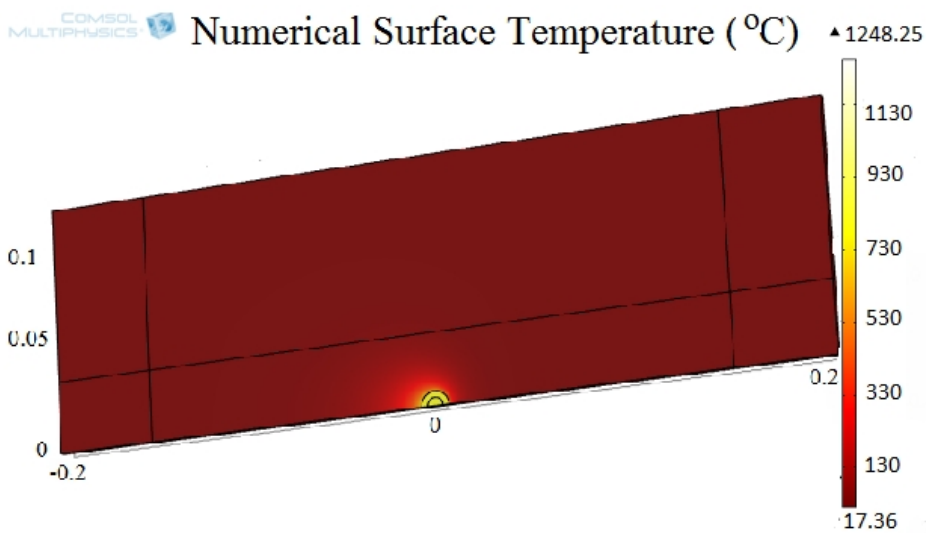

Figure 5-18: Numerical temperature surface plot for Titanium

The maximum temperature reached by the workpiece as predicted by the model is calculated to be 1248.25 °C which is approximately 75% of the melting point of Titanium (±1600 °C) which agrees with expected results for peak temperatures of Ti 6Al-4V [33]. From both

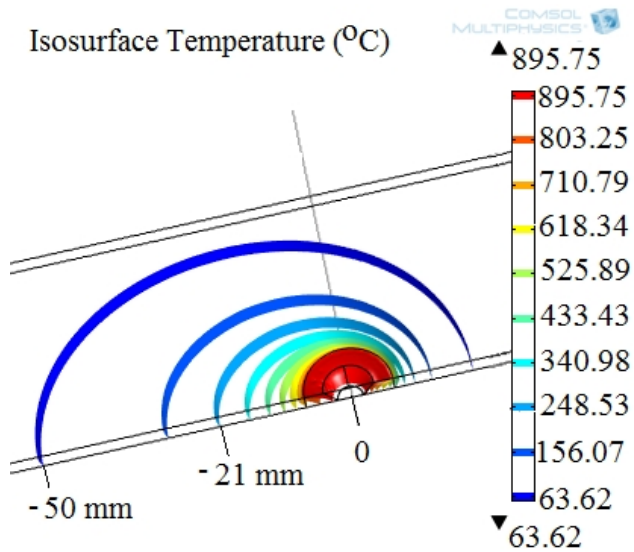

Figure 5-19: Temperatures along isosurfaces for Titanium

Figures (5-18) and (5-19), it can be noted that although the temperatures are higher around the tool for Titanium than for Aluminium, the region with the highest temperatures is far more concentrated around the tool. All the temperatures higher than 220 °C are found within a 20 mm radius around the tool for Titanium while the temperatures higher than 220 °C in the Aluminium workpiece were generally found to be within a 50 mm radius of the tool. This is to be expected since the thermal conductivity values for Titanium (± 20 W/(m.K)) are much lower than that of Aluminium (± 180 W/(m.K)).

5.3.2 Model Validation

Figure (5-20) compares the temperature results for thermocouple positions 1, 2 and 3 in Figure (4-8).

The maximum temperatures obtained at the three thermocouples at positions 1, 2 and 3

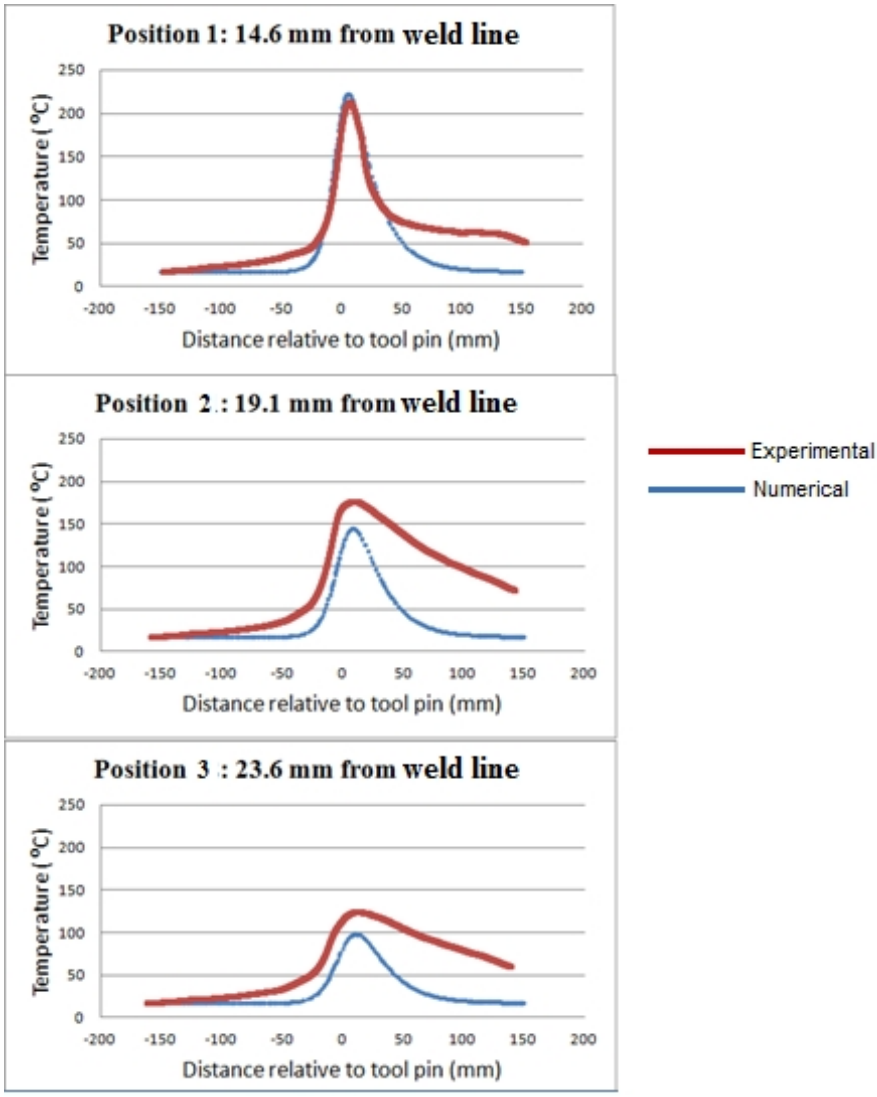

Figure 5-20: Temperatures for Titanium at positions 1, 2 and 3

are compared to the maximum temperatures predicted for the corresponding positions in the numerical model. These are given in Figure (5-21).

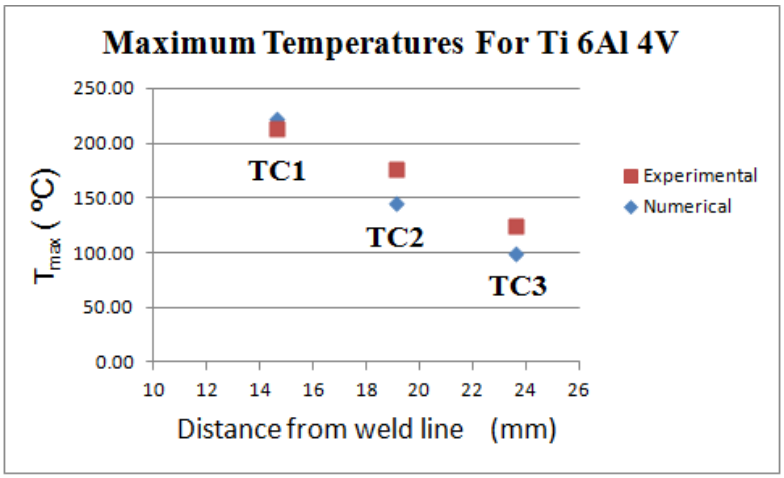

Figure 5-21: Maximum temperatures for Titanium thermocouples positions 1, 2 and 3

As in the results of Al 6082-T6, Figures (5-20) and (5-21) show the expected trend of the maximum temperature becoming lower with position away from the weld center line. Contrary to the Aluminium results, however, the numerical estimations become more accurate nearer to the weld line. Figure (5-21), it is clear that the model slightly over estimates the temperature near the weld line but underestimates it further away. This could be due to the fact that the thermal conductivity function is faulty or the numerical mesh is too coarse. The maximum temperature measured at the thermocouple closest to the tool (14.6 mm from weld line) for the Titanium weld was 212.8 ^{o}C which is 12.8% of the melting point. This is too low to give a good estimation of the maximum temperatures around the tool but can still be used for the model validation.

5.3.3 Error Analysis

The error involved in estimating the maximum temperature at thermocouple positions 1, 2 and 3, $e^{\max}$ was calculated using Equation (5.2) while the error involved in estimating temperature trend as a whole, e^{area}, was calculated using Equation (5.3). The following table shows the results for these errors:

	TC1	**TC2**	**TC3**
$\mathbf{e}^{\max}$	4.7%	18.1%	21.0%
$\mathbf{e}^{\text{area}}$	25.3%	52.4%	49.0%

Table 5.4: Relative error in temperature prediction for Titanium

The error values suggest that the maximum temperature prediction is in reasonable agreement with the experimental results since on average, $\mathbf{e}^{\max}$ is 14.6%, although the error is larger at positions 2 and 3. The errors involved in predicting the overall trend are, however very large. This could suggest that the model is not as well suited to Titanium as it is for Aluminium. The heat flux term selected from Hattel and co-workers [25] (see Equation (3.8)) was originally applied to Aluminium which is a softer material than Titanium. It could be that this heat flux term is not as well suited to harder materials such as Titanium. The fact that $e_{\max}$ and $\boldsymbol{e}_{\text{area}}$ get larger as the thermocouple positions are further away from the weld center line is opposite to the Aluminium results. The increase in error with distance away from the tool could be due to the heat transfer coefficient used at the plate-backing plate interface. This value is the same value used in the Aluminium model and so could be overestimating the amount of heat flowing into the backing plate from the Titanium. Since the backing plate used in the Titanium welding is made of a material that is not a very good conductor, the boundary condition at

the bottom of the welding plate could be set to an insulation condition which might increase the accuracy of the temperature prediction. This was attempted but the Titanium model was found to be very sensitive to this change. Further work needs to be done in order to improve this boundary condition in the future.

5.3.4 Tool Surface Temperatures

The predicted temperatures at three points, A (at the tool shoulder edge), B (at the top of the pin) and C (at the bottom of the pin) on the tool surface have been shown on the temperature plot for the region around the tool in Figure (5-22).

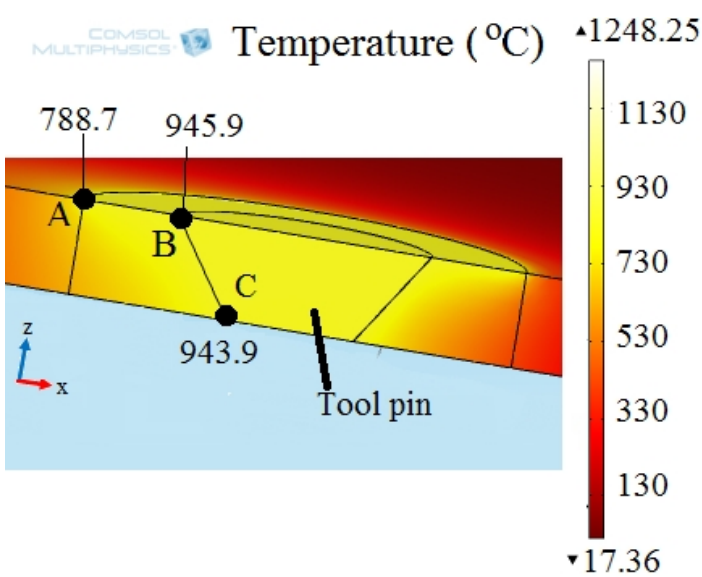

Figure 5-22: Tool surface temperatures for Titanium

The corresponding predicted temperatures for points A, B and C are 788.7 °C, 945.0 °C and 943.9 °C respectively. The temperatures are lower than expected results found by other researchers [33, 54] in which temperatures around the tool were closer to 1000 °C. The lower

than expected temperatures could be due to the heat transfer coefficient used between the backing plate and the workpiece in the model that is allowing for the escape of too much heat. The material used for backing plate acts almost as an insulator which allows very little heat to escape. For this reason, the model could possibly be improved if a symmetry boundary condition was employed at the bottom of the workpiece instead of a heat conduction condition. The symmetry condition simulates the insulation condition in reality.

Since the flux term at the pin surface depends on the radius of the pin, the results, as expected, show that the predicted temperature at the bottom of the tool pin is lower than that at the top of the pin. The temperature difference between points B and C is only 2 ^{o}C, however, which is very small in relation to the temperatures at B and C. This could be explained by the fact that in comparison to the magnitude of the rotational speed and the shear stress in the heat flux term, the radius is very small thus only slightly influencing the temperature difference. Another reason for this could be that the extrusion of the computational mesh from the top surface to the bottom was not fine enough.

5.3.5 Contour Plots for All Twelve Thermocouples

As done for the results of Aluminium, the numerical and experimental results of the twelve thermocouples now also need to be compared in order to determine the accuracy of the model as a whole. Figures (5-23) and (5-24) show the contour plots for the thermocouples where the values on the y-axis represent the distance of the thermocouple position from the weld line and the values on the x-axis show the distance from the left side of the workpiece using Figure (5-18)) as a reference. The x and y co-ordinates (in mm) of the thermocouple positions on the contour plots are given in Table (5.5). The table also shows the predicted temperature ($\mathbf{T}_{\text{model}}$) and the

experimental temperature ($\mathbf{T}_{\text{exp}}$) at the corresponding thermocouple position. The error was calculated using Equation (5.1). The plots were generated by interpolating the temperatures between the values obtained at the thermocouple positions. For the experimental results, this was done for the instant in time when thermocouple 1 has its maximum temperature.

	1	**2**	**3**	**4**	**5**	**6**	**7**	**8**	**9**	**10**	**11**	**12**
x (mm)	150	150	150	130	130	130	110	110	110	90	90	90
y (mm)	14.6	19.1	23.6	14.6	19.1	23.6	14.6	19.1	23.6	14.6	19.1	23.6
$\mathbf{T}_{\text{model}}$ (^{o}C)	40.1	37.3	34.2	77.4	67.1	56.8	166.2	125.0	92.0	193.0	119.7	79.1
$\mathbf{T}_{\text{exp}}$ (^{o}C)	142.1	136.8	108.1	186.4	162.4	123.4	226.3	216.7	28.2	212.8	159.9	99.8
e	71.7	72.7	68.3	58.5	58.8	54.0	26.6	42.3	226.1	9.3	25.1	20.7

Table 5.5: Errors for temperatures at thermocouple co-ordinates for Titanium

Unlike the contour plots for Aluminium, the numerical contour plot for Titanium does not have a similar appearance to the experimental plot. This suggests that the model is not as accurate in estimating the temperatures involved in the FSW of Titanium than it is for Aluminium. The maximum temperature for the numerical temperature plot occurs at position 1 while the maximum temperature in the experimental plot occurs closer to position 4. The temperatures predicted by the model are also much lower than the experimental results (between 20 to 100 ^{o}C). The reason that the numerical plot does not predict the experimental plot very well can possibly be explained due to the steady-state nature of the numerical temperature prediction. Unlike in the Aluminium welds, the thermocouples were placed closer to the start of the weld where the transient heating effects have a larger influence on the temperatures of the workpiece. The model predicts the temperatures at the instant in time when thermocouple

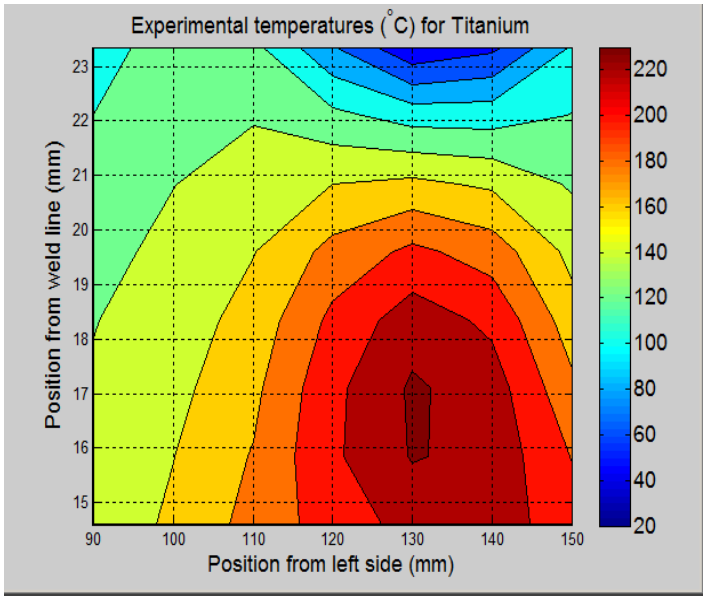

Figure 5-23: Contour plot for experimental thermocouple readings for Titanium

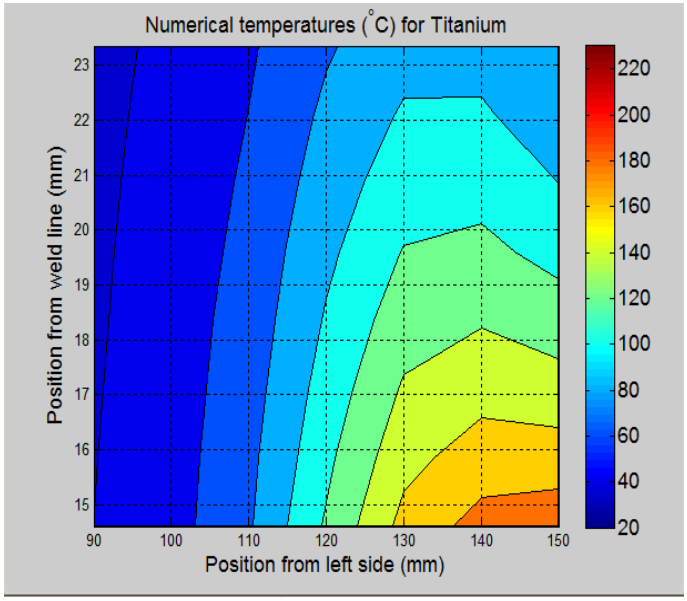

Figure 5-24: Numerical contour plot for thermocouple positions for Titanium

1 has reached its maximum. Since the model is time-independent, this is also the same instant at which thermocouple 1 has the highest temperature among all twelve thermocouples. When the experimental results were analyzed, it was noted that due to transient heating effects of the thermocouples in the wake of the tool, the temperature at thermocouple 1 was never the maximum out of all twelve thermocouples. A better comparison between the model and the experimental results can be performed in the future if the thermocouples are placed at positions where they are placed further away from the start of the weld. The reason that the numerical temperature is lower than the experimental results could again be due to the heat transfer coefficient used or the heat conduction boundary condition assumed at the workpiece-backing plate interface.

These contour plots and corresponding error values suggest that the Titanium model is not as accurate as the Aluminium model. The heat flux term used in the model could possibly be more suited to softer materials such as Aluminium than for harder materials such as Titanium.

Chapter 6

Conclusions and Future work

6.1 Conclusions

This study forms part of a larger numerical modelling project for FSW in which the thermal model forms the foundation. A purely thermal FEM model was developed in order to predict the steady-state temperatures that occur in the workpiece during FSW. Finite element analysis proved to be a good choice of numerical method, since complicated natural boundary conditions and the tool geometry could be implemented without difficulty. COMSOL Multiphysics [29] software was used for the implementation of the model and was found to be very user friendly and used minimal computational time (± 5 min) when solving the heat transfer problem.

Based on the model of Song and Kovacevic [38], the model assumed a stationary FSW tool with a moving workpiece for the case of Aluminium Al 6082-T6. For this reason, an artificial convection term was added to the heat equation and rotational speeds were included in the boundary conditions. This approach proved to be useful in capturing the effects of a moving tool without the difficult task of modelling a moving heat source. This effect can be visualized

in the temperature wake around the tool in Figure (5-1).

The domain geometry was also selected from the model developed by Song and Kovacevic [38]. The model employed 50 000 to 100 000 degrees of freedom in the computational mesh without any noticeable change to the results which implies that the choice of mesh size for the model was appropriate.

The heat generation was modelled as a heat flux boundary condition at the tool-workpiece interface rather than an internal heat source. The heat generation was assumed to be due to plastic deformation and friction. The heat flux term used in the model was selected from the work of Hattel and co-workers [25] since it had no dependence on estimated frictional coefficients which could be a source of error. The effects of friction were still however included indirectly in the heat flux term by including the temperature dependent shear stress for the workpiece material (see Equation (3.8)).

When the model was applied to Aluminium Al 6082-T6, the predicted temperatures were found to be in good agreement with the experimental results since the calculated errors involved were approximately 15% or less. The maximum temperatures at thermocouple positions were however slightly underestimated ($\pm$10 to 20 ^{o}C) for the five welding conditions. The maximum temperature of the workpiece was predicted to be approximately 400 ^{o}C under the tool shoulder at the tool pin radius.

A parametric study was performed on the Aluminium model and the following conclusions were made about temperatures on the workpiece at the tool-workpiece interface:

- Temperature increases with increasing rotational speeds,
- Temperature increases with decreasing feed rates at positions on the tool pin,

- Rotational speed has a greater effect on the temperature than the feed rate, and
- Lower rotational speeds (300 to 660 rpm) have a greater effect on the change in the maximum predicted temperature of the workpiece than higher rotational speeds (840 to 1200 rpm).

The model, when applied to Titanium Ti 6Al-4V, was found to be much less accurate than the Aluminium model when compared to the experimental results since error values were calculated to be more than 15%. The heat flux term used in this model could be more suited to softer materials but cannot be disregarded completely since there is not enough experimental data to support this. The predicted temperatures on the surface of the workpiece at the tool-workpiece interface ranged from approximately 785 ^{o}C at the radius of the shoulder to 946 ^{o}C at the pin radius.

From the error analysis performed on both the Aluminium and Titanium models, it can be concluded that the model is more accurate in predicting the maximum temperature at a location than the overall temperature trend at that point.

6.2 Future Work

The following recommendations can be made to improve the model.

1. Thermocouples should be placed closer to the weld line or infrared cameras should be used to measure the temperature near the tool in order to better validate the model.
2. Since FSW is a highly coupled problem where the heat generation is highly dependent on the material flow of the workpiece and vice versa, future work should be done in

determining how a thermo-mechanical or a thermo-fluid model could improve on the results in this study. This will also aid in predicting properties such as residual stress which also influences the quality of the weld.

3. A study should be done to determine whether a direct dependence on friction and frictional coefficients in the heat generation term could aid in making the Titanium model more accurate.

4. Numerical methods such as FDM and meshless methods should be investigated as an alternative to FEM.

5. For the Titanium model, changing the boundary condition between the workpiece and backing plate could improve the accuracy of the model. This could be done in one of two ways, namely, a conduction condition but with a different heat transfer coefficient, or, adding an insulation/ symmetry boundary condition at the interface.

6. Inverse methods should be studied with the aim to obtain parameters such as the heat transfer coefficient from experimental results.

7. Spatially dependent heat transfer coefficients could be employed throughout the workpiece.

8. Optimization techniques, such as the use of genetic algorithms, will also be investigated in order to use the model to optimize tool geometry and welding conditions.

6.3 Nomenclature

ρ : Material density [kg/m^3]

c : Specific heat [J/(kg.K)]

k : Thermal Conductivity [W/(m.K)]

T : Temperature [K]

Q : Net heat generated per unit volume [J/m^3]

q : Total heat flux [J/m^3]

ω : Angular velocity of the tool [rad/s]

r : Radial distance from the center of the tool pin to calculation point [m]

τ_{yield} : Temperature dependent shear stress [N/m^2]

σ_{yield} : Maximum temperature dependent yield stress [N/m^2]

h_{air}: Heat transfer coefficient between aluminium and air [W/(m^2.K)]

ϵ : Surface emissivity

σ : Stefan-Boltzmann constant [W/(m^2.K^4)]

T_0 : Initial plate temperature [K]

h_{steel}: Heat transfer coefficient between aluminium and steel [W/(m^2.K)]

r_{pin} : Radius of the tool pin [m]

V : Unit volume [m^3]

μ : Coefficient of friction

R : Surface radius

N : Rotational speed [rad/s]

P : Pressure across interface [N/m^2]

v_{weld} : Translational speed of the tool [m/s]

F_n : Normal force [N]

F : Body forces [N]

σ : Cauchy stress tensor [N/m^2]

u : Displacement [m]

C : Fourth order stiffness tensor [N/m]

ε : Infinitesimal strain tensor

v : Velocity [m/s]

η : Dynamic viscosity [N.s/m^2]

Bibliography

[1] W. M. Thomas, E. D. Nicholas, J. C. Needham, M. G. Murch, P. Temple-Smith, and C. J. Dawes, "Improvements relating to friction stir welding," in *European Patent Specification 0615 480 B1*, 1991.

[2] W. Thomas, P. Threadgill, and E. Nicholas, "Feasibility of friction stir welding steel," *Science and Technology of Welding & Joining*, vol. 4, no. 6, pp. 365–372, 1999.

[3] P. A. Colegrove and H. R. Shercliff, "3-Dimensional CFD modelling of flow round a threaded friction stir welding tool profile," *Journal of Materials Processing Technology*, vol. 169, pp. 320 – 327, 2005.

[4] M. Mashinini, "Process window for Friction Stir Welding of 3 mm Titanium (Ti-6Al-4V)," Master's thesis, Nelson Mandela Metropolitan University, 2010.

[5] M. Attallah, *Friction Stir Welding of Aluminium Alloys.* Lambert Academic Publishing, 2011.

[6] R. Kumar and R. Singh, "Effect of Friction Stir Welding on Mechanical Properties of Dissimilar Aluminium Alloys," in *National Conference on Innovative Paradigms in Engineering and Technology*, 2012.

[7] G. C. M. Vural, A. Ogur and C. Ozarpa, "On the friction stir welding of aluminium alloys EN AW 2024-0 and EN AW 5754-H22," *Archives of Materials Science and Engineering*, vol. 28, pp. 49–54, 2007.

[8] Y. Hwang, P. Fan, and C. Lin, "Experimental study on Friction Stir Welding of copper metals," *Journal of Materials Processing Technology*, vol. 210, no. 12, pp. 1667 – 1672, 2010.

[9] W.-B. Lee, C.-Y. Lee, W.-S. Chang, Y.-M. Yeon, and S.-B. Jung, "Microstructural investigation of friction stir welded pure titanium," *Materials Letters*, vol. 59, no. 26, pp. 3315 – 3318, 2005.

[10] C. Blignault, "Design, Development and Analysis of the Friction Stir Welding process," Master's thesis, Nelson Mandela Metropolitan University, 2002.

[11] R. Mishra and M. Mahoney, *Friction Stir Welding and Processing.* ASM International, 2007.

[12] Ø. Frigaard, Ø. Grong, and O. T. Midling, "A process model for friction stir welding of age hardening aluminum alloys," *Metallurgical and Materials Transactions A*, vol. 32, no. 5, pp. 1189–1200, 2001.

[13] S. Geurdoux, "Numerical Simulation of the Friction Stir Welding Process," Ph.D. dissertation, Mines de Paris, 2007., 2007.

[14] P. Withers, "Friction Stir Welding of aluminium alloys," *International Materials Reviews*, vol. 54, pp. 49–53, 2009.

[15] Z. Georgeou, "Analysis of Material Flow Around a Retractable Pin in a Friction Stir Weld," Master's thesis, Port Elizabeth Technikon, 2003.

[16] H. K. Mohanty, M. M. Mahapatra, P. Kumar, P. Biswas, and N. R. Mandal, "Effect of tool shoulder and pin probe profiles on friction stirred aluminum welds - a comparative study," *Journal of Marine Science and Application*, vol. 11, pp. 200–207, 2012.

[17] H. Lombard, "Optimized Fatigue and Fracture Performance of Friction Stir Welded Aluminium Plate: A Study of the Inter-relationship Between Process Parameters, TMAZ, Microstructure, Defect Population and Performance," Ph.D. dissertation, University of Plymouth, 2007.

[18] T. Khaled, "An Outsider Looks at Friction Stir Welding," Federal Aviation Adminisration, Tech. Rep., 2005.

[19] H. Schmidt and J. Hattel, "Thermal modelling of friction stir welding," *Scripta Materialia*, vol. 58, no. 5, pp. 332 – 337, 2008.

[20] B. Rajamanickam, "Numerical Simulation of Transient Temperature in Friction Stir Welding of Aluminum Alloy 2014 -T6," *Manufacturing Engineering*, vol. 2, pp. 41–44, 2007.

[21] Y. J. Chao, X. Qi, and W. Tang, "Heat Transfer in Friction Stir Welding - Experimental and Numerical Studies," *Journal of Manufacturing Science and Engineering*, vol. 125, no. 1, p. 138, 2003.

[22] P. Colegrove, "3 Dimensional Flow and Thermal Modelling of the Friction Stir Welding Process," Ph.D. dissertation, University of Adelaide, 2001.

[23] J. F. Lancaster, *Metallurgy of welding*, 6th ed., W. Andrew, Ed. Woodhead Publishing, 1999.

[24] J. L. Covington, "Experimental and Numerical Investigation of Tool Heating During Friction Stir Welding," Master's thesis, Brigham Young University, 2005.

[25] J. Hattel, H. Schmidt, and C. Tutum, "Thermomechanical Modelling of Friction Stir Welding," in *Trends in Welding Research*, 2009.

[26] C. M. Chen and R. Kovacevic, "Finite element modeling of friction stir welding-thermal and thermomechanical analysis," *International Journal of Machine Tools and Manufacture*, vol. 43, no. 13, pp. 1319 – 1326, 2003.

[27] T. De Vuyst, "Finite Element Modelling of Friction Stir Welding of Aluminium alloy Plates - Inverse Analysis using a Genetic Algorithm," *Welding in the World*, vol. 49, p. 12, 2005.

[28] P. A. Colegrove, "Modelling the Heat Generation , Temperature and Microstructure of Friction Stir Welds using Comsol Multiphysics," in *COMSOL Users Conference 2006 Birmingham*, 2006.

[29] *COMSOL Multiphysics 4.3a User's manual*, Comsol inc., Burlington Massechusetts, 2012.

[30] J. Battaglia, *Heat Transfer in Materials Forming Processes*. John Wiley & Sons, 2008.

[31] A. Bejan, *Heat transfer*. John Wiley & Sons, Inc., 1993.

[32] H. C. Rogers, "Adiabatic Plastic Deformation," *Annual Review of Materials Science*, vol. 9, no. 1, pp. 283–311, 1979.

[33] R. Mishra and M. Mahoney, *Friction Stir Welding and Processing.* ASM International, 2007.

[34] X. Qin, "Thermo-elasto-visco-plastic modelling of friction stir welding in an Eulerian reference frame," Ph.D. dissertation, Pensylvania State University, 2009.

[35] R. Nandan, G. Roy, and T. Debroy, "Numerical simulation of three-dimensional heat transfer and plastic flow during friction stir welding," *Metallurgical and Materials Transactions A*, vol. 37, pp. 1247–1259, 2006.

[36] X. Deng and S. Xu, "Two-Dimensional Finite Element Simulation of Material Flow in the Friction Stir Welding Process," *Journal of Manufacturing Processes*, vol. 6, no. 2, pp. 125 – 133, 2004.

[37] Y. J. Chao and X. Qi, "Thermal and thermo-mechanical modeling of friction stir welding of aluminum alloy 6061-T6," *Journal of materials processing manufacturing science*, vol. 7, no. 2, pp. 215–233, 1998.

[38] M. Song and R. Kovacevic, "Thermal modeling of friction stir welding in a moving coordinate system and its validation," *International Journal of Machine Tools and Manufacture*, vol. 43, no. 6, pp. 605 – 615, 2003.

[39] M. Maalekian, E. Kozeschnik, H. Brantner, and H. Cerjak, "Comparative analysis of heat generation in friction welding of steel bars," *Acta Materialia*, vol. 56, no. 12, pp. 2843 – 2855, 2008.

[40] G. Totten, *Handbook of Residual Stress and Deformation of Steel.* A S M International, 2002.

[41] D. Kim, H. Badarinarayan, J. H. Kim, C. Kim, K. Okamoto, R. Wagoner, and K. Chung, "Numerical simulation of friction stir butt welding process for AA5083-H18 sheets," *European Journal of Mechanics - A/Solids*, vol. 29, no. 2, pp. 204 – 215, 2010.

[42] G. Batchelor, *An introduction to fluid dynamics*, ser. Cambridge mathematical library. Cambridge University Press, 2000.

[43] R. Nandan, G. Roy, T. Lienert, and T. Debroy, "Three-dimensional heat and material flow during friction stir welding of mild steel," *Acta Materialia*, vol. 55, no. 3, pp. 883 – 895, 2007.

[44] Z. Zhang and H. Zhang, "Numerical studies on controlling of process parameters in friction stir welding," *Journal of Materials Processing Technology*, vol. 209, no. 1, pp. 241 – 270, 2009.

[45] C. Hirt, "An arbitrary Lagrangian-Eulerian computing technique," in *Proceedings of the Second International Conference on Numerical Methods in Fluid Dynamics*. Springer Berlin / Heidelberg, 1971, vol. 8, pp. 350–355.

[46] J. Hilgert, H. N. B. Schmidt, J. F. dos Santos, and N. Huber, "Thermal Models for Bobbin Tool Friction Stir Welding," *Journal of Materials Processing Technology*, vol. 211, pp. 197–204, 2010.

[47] R. Nandan, T. Debroy, and H. K. Bhadeshia, "Recent Advances in Friction Stir Welding - Process, Weldment Structure and Properties," *Process in Materials Science*, vol. 53, pp. 980–1023, 2008.

[48] A. F. Bower, *Applied Mechanics of Solids*, Taylor and F. Group, Eds. CRC Press, 2010.

[49] A. Larsen, M. Stolpe, and J. H. Hattel, "Estimating the workpiece-backingplate heat transfer coefficient in friction stirwelding," *Engineering Computations*, vol. 29, no. 1, pp. 65–82, 2012.

[50] R. Lewis, P. Nithiarasu, and K. Seetharamu, *Fundamentals of the Finite Element Method for heat and fluid flow.* Wiley, 2004.

[51] H. B. R. Rai, A. De and T. DebRoy, "Review on Friction Stir Welding Tools," *Science and Technology of Welding and Joining*, vol. 16, p. 325, 2011.

[52] K. Oyedemi, "Increasing the gap tolerance in friction stir welded joints of AA 6082-T6," Master's thesis, Nelson Mandela Metropolitan University, 2012.

[53] C. Owen, "Two Dimensional Friction Stir Welding Model with Experimental Validation," Master's thesis, Brigham Young University, 2006.

[54] P. Edwards and M. Ramulu, "Peak temperatures during friction stir welding of Ti 6Al-4V," *Science and Technology of Welding and Joining*, vol. 15, p. 468, 2010.

[55] J. Wong, "The Correspondence between Experimental Data and Computer Simulation of Friction Stir Welding (FSW)," Master's thesis, West Virginia University, 2008.